MCB
Journals.ASM.org

PEA15 Regulates the DNA Damage-Induced Cell Cycle Checkpoint and Oncogene-Directed Transformation

Arvindhan Nagarajan,[a] Shaillay Kumar Dogra,[b] Alex Y. Liu,[a] Michael R. Green,[c] Narendra Wajapeyee[a]

Department of Pathology, Yale University School of Medicine, New Haven, Connecticut, USA[a]; Singapore Institute of Clinical Sciences, Agency for Science Technology and Research, Brenner Center for Molecular Medicine, Singapore, Singapore[b]; Howard Hughes Medical Institute, Programs in Gene Function and Expression and Molecular Medicine, University of Massachusetts Medical School, Worcester, Massachusetts, USA[c]

Regulation of the DNA damage response and cell cycle progression is critical for maintaining genome integrity. Here, we report that in response to DNA damage, COPS5 deubiquitinates and stabilizes PEA15 in an ATM kinase-dependent manner. PEA15 expression oscillates throughout the cell cycle, and the loss of PEA15 accelerates cell cycle progression by activating *CDK6* expression via the c-JUN transcription factor. Cells lacking PEA15 exhibit a DNA damage-induced G_2/M checkpoint defect due to increased CDC25C activity and, consequentially, higher cyclin-dependent kinase 1 (CDK1)/cyclin B activity, and accordingly they have an increased rate of spontaneous mutagenesis. We find that oncogenic RAS inhibits PEA15 expression and that ectopic PEA15 expression blocks RAS-mediated transformation, which can be partially rescued by ectopic expression of CDK6. Finally, we show that PEA15 expression is downregulated in colon, breast, and lung cancer samples. Collectively, our results demonstrate that tumor suppressor PEA15 is a regulator of genome integrity and is an integral component of the DNA damage response pathway that regulates cell cycle progression, the DNA-damage-induced G_2/M checkpoint, and cellular transformation.

The conversion of a normal cell to a cancer cell requires multiple genetic and epigenetic alterations. These changes include the activation of oncogenes and inactivation of tumor suppressor genes. Although oncogenes are expected to exert proliferative effects, paradoxically, introduction of an oncogene in primary mouse or human cells can induce a state similar to replicative senescence, which is referred to as oncogene-induced senescence.

Oncogene-induced senescence is a mechanism that is believed to prevent neoplastic transformation (1, 2). Cells undergoing oncogene-induced senescence display characteristic hallmarks of replicative senescence (3) but with a much more rapid onset. Several mechanisms of oncogene-induced senescence have been proposed (3). One of the proposed mechanisms is that oncogenes can cause DNA replication stress, which activates the DNA damage response (DDR) pathway, leading to oncogene-induced senescence (4, 5). These studies suggest that proteins that mediate oncogene-induced senescence might also regulate the DNA damage response pathway and thereby function as tumor suppressors. In good agreement with this view, tumor suppressor proteins, such as p53, that play an important role in oncogene-induced senescence have been shown to regulate DNA damage checkpoints and DNA repair to maintain genome integrity, a function that is necessary for p53 to prevent neoplastic transformation (6–8).

We previously performed a genome-wide RNA interference (RNAi) screen for mediators of oncogenic BRAF-induced cellular senescence (9) and identified 17 genes. One of the genes identified from our RNAi screen was the protein enriched in astrocytes 15 (PEA15). PEA15 is a multifunctional protein that has been implicated in diverse biological processes and regulates several signaling pathways (10). Notably, PEA15 has been shown to block extracellular signal-regulated kinase (ERK)-dependent transcription and proliferation by binding ERK and preventing its localization to the nucleus (11). Accordingly, genetic deletion of PEA15 results in increased ERK nuclear localization, leading to enhanced transcription of ERK target genes and proliferation (11).

Here, we show that PEA15 functions as a tumor suppressor by promoting the DNA damage-induced G_2/M checkpoint, regulating cell cycle progression, and inhibiting RAS-mediated transformation. In addition, we find that PEA15, like other tumor suppressors, is epigenetically silenced in human tumors.

MATERIALS AND METHODS

Cell culture, plasmids, and cloning. Human diploid fibroblast, HCT116, HeLa, U2OS, SKMEL-28, and MCF7 cell lines were obtained from ATCC and maintained as recommended by ATCC. Mouse embryonic fibroblast (MEF)/SV40-ER and immortalized MEL-ST cells were a kind gift of Qin Yan (Yale University) and Robert Weinberg (Massachusetts Institute of Technology), respectively. The *PEA15* gene was cloned into pEGFP-C1 (where EGFP is enhanced green fluorescent protein) (Life Technologies) between EcoRI and BamHI to generate a *GFP-PEA15* fusion gene. *CDK6* was cloned into pCDNA3.1 (Life Technologies). MYC-COPS5 cloned in pCDNA3 (a kind gift from Joseph R. Nevins) was subcloned into pCDNA3.1 (Life Technologies) between HindIII and XhoI. To generate glutathione *S*-transferase (GST)–COPS5, COPS5 was cloned into pGEX4T-1 (GE Healthcare) between the EcoRI and XhoI sites. The COPS5-D151N JAMM (JAB1/MPN/Mov34 metalloenzyme) domain mutant and COPS5-T154A and COPS5-S320A were generated by site-directed mutagenesis using a QuikChange XL kit (Agilent Technologies), and mutants were confirmed by DNA sequencing and immunoblot analysis. The following primers were used for site-directed mutagenesis of COPS5: for COPS5-D151N, 5′-GCTGGCTTTCTGGGATTAATGTTAG TACTCAGATGCT-3′ (forward) and 5′-AGCATCTGAGTACTAACATT AATCCCAGAAAGCCAGC-3′ (reverse); COPS5-T154A, 5′-CTGGGATT GATGTTAGTGCTCAGATGCTCAATCAGC-3′ (forward) and 5′-GCTGATT GAGCATCTGAGCACTAACATCAATCCCAG-3′ (reverse); COPS5-S320A,

Received 21 November 2013 Returned for modification 19 December 2013
Accepted 31 March 2014
Published ahead of print 7 April 2014
Address correspondence to Narendra Wajapeyee, narendra.wajapeyee@yale.edu.

doi:10.1128/MCB.01542-13

5′-CTATCCATGGATTGATGGCTCAGGTTATTAAGGA-3′ (forward) and 5′-TCCTTAATAACCTGAGCCATCAATCCATGGATAG-3′ (reverse).

RT-qPCR and ChIP assays. Total RNA was extracted using TRIzol (Life Technologies) and purified using an RNeasy minikit (Qiagen). cDNA was generated using a ProtoScript First-Strand cDNA synthesis kit (New England BioLabs). Quantitative PCR was then performed using the Power SYBR green 2× master mix (Life Technologies). All reverse transcription-quantitative PCRs (RT-qPCRs) were performed in triplicates. The following primers were used for RT-qPCR: for *PEA15*, 5′-CTAGGGGAGGGGGCTGAGTT-3′ (forward) and 5′-GGTGGGGGTTGAGTGGTCTC-3′ (reverse); *CDC25C*, 5′-CAGTGGCTGCCTTACTGTCG-3′ (forward) and 5′-AAAGGGACGATGGGCTTCTT-3′ (reverse); *COPS5*, 5′-AACTGGCCAACAACATGCAG-3′ (forward) and 5′-CTGGCATGCATCACCATCTT-3′ (reverse); *CDK6*, 5′-GCGCCTATGGGAAGGTGTTC-3′ (forward) and 5′-CTGTGCCCAGCATCAGGAAC-3′) (reverse); *COPS1*, 5′-GAGTCCACCCCAGAGATTGC-3′ (forward) and 5′-GGACAGCACTCAGGGAAGT-3′ (reverse); *COPS3*,5′-TCCCATCTGGACACTGTGCT-3′ (forward) and 5′-CGAATGTGCTCCCCATTACA-3′ (reverse); *COPS6*, 5′-ACAGCAACAGGCAGTGGAGA-3′ (forward) and 5′-CCGGGAGACAGTGACACAGA-3′ (reverse); *USP15*, 5′-CCCAGGTGCATCCAATTTTT-3′ (forward) and 5′-AGGCCTGGCTGTTCATTGTT-3′ (reverse); *ACTIN*, 5′-GCATGGAGTCCTGTGGCATC-3′ (forward) and 5′-TTCTGCATCCTGTCGGCAAT-3′ (reverse). The relative fold changes in mRNA expression levels were calculated using comparative threshold cycle (C_T) method (12). The amount of target gene expression under individual conditions was normalized to the expression of the human β-*ACTIN* gene, which was used as the internal control. Relative gene expression among treatment conditions was calculated using the formula $2^{-\Delta\Delta CT}$. PCR efficiency of target genes was matched with PCR efficiency of β-*ACTIN* by ensuring that the log input versus ΔC_T had a slope of zero. Chromatin immunoprecipitation (ChIP) experiments were performed as described previously (13). Briefly, paraformaldehyde-fixed cells were lysed in SDS lysis buffer (1% SDS, 50 mM Tris-HCl [pH 8.0], 10 mM EDTA, and protease inhibitor cocktail [Roche]) and sonicated at 4°C. The lysate was diluted with ChIP buffer (0.01% SDS, 1.1% Triton X-100, 1.2 mM EDTA, 16.7 mM Tris-HCl [pH 8.0], 16.7 mM NaCl, and protease inhibitor cocktail [Roche]), and chromatin immunoprecipitation was performed by incubating the sample with antibody against c-JUN (Cell Signaling), followed by immobilization on protein A/G-agarose beads (Life Technologies). The chromatin was eluted, and DNA was extracted following phenol-chloroform treatment. Quantitative PCR (qPCR) was performed using cyclin-dependent kinase 6 (CDK6) promoter primers (forward, 5′-GAGGGTAGCGGCGCAACA-3′; reverse, 5′-CCTCGGGGATGAGCGAGC-3′). Fold enrichment was calculated as the ratio of immunoprecipitated DNA to input DNA.

shRNAs, siRNAs, transfection, retrovirus, lentivirus preparation, immunoblotting, cell fractionation cycloheximide chase, and karyotyping. *PEA15*, *COPS5*, *COPS3*, *COPS6*, *USP15*, *CDC25C*, *CDK6*, and control short hairpin RNAs (shRNAs) were obtained from Open Biosystems. The product identifications for these shRNAs are as following: *PEA15*, TRCN0000059389 and TRCN0000059391; *COPS5*, TRCN0000019200 and V3LHS_361325; *CDC25C*, TRCN0000002433 and TRCN0000002434; *CDK6*, TRCN0000000486 and TRCN0000000488; *COPS1*, TRCN0000036864 and TRCN0000036865; *COPS3*, TRCN0000154961 and TRCN0000151054; *COPS6*, TRCN0000072561 and TRCN0000072562; *USP15*, TRCN0000007568 and TRCN0000007569. c-*JUN* (VHS40918) and control small interfering RNAs (siRNAs) were obtained from Ambion. Lentivirus particles were prepared by cotransfecting the shRNA plasmids and lentiviral packaging plasmids pSPAX2 and pMD2.G into 293T cells using Effectene (Qiagen). Retrovirus particles were prepared as described previously (9). Immunoblot analysis was performed as described previously (14). Nuclear and cytoplasmic fractionations were prepared as described previously (14). Protein concentrations were estimated using a Bradford protein assay kit (Bio-Rad). The following antibodies were used for immunoblot analyses: total ERK1/2 (Cell Signaling), phospho-ERK1/2 (Cell Signaling), PEA15 (Santa Cruz Biotechnology), COPS5 (Santa Cruz Biotechnology), COPS1 (Santa Cruz Biotechnology), COPS6 (Santa Cruz Biotechnology), CDK6 (Santa Cruz Biotechnology), β-actin (Sigma), CDK1 (Cell Signaling), cyclin B1 (Santa Cruz Biotechnology), phospho-CDK1 (Cell Signaling), CDC25C (Cell Signaling), phospho-CDC25C (Cell Signaling), total ATM (Cell Signaling), phospho-ATM (Cell Signaling), c-JUN (Cell Signaling), phospho-SQ (Cell Signaling), 5-methylcytidine (Eurogentec), and p27 (Santa Cruz Biotechnology) antibodies.

For cycloheximide chase experiments, cycloheximide was added immediately after gamma irradiation or with etoposide or doxorubicin at a final concentration of 50 μg/ml. Whole-cell lysates were prepared at 0, 4, 8, 16, and 32 h after gamma irradiation or after treatment with etoposide or doxorubicin. Immunoblotting of PEA15 and actin proteins was performed. The intensity of the protein bands was quantified using ImageJ software (National Institutes of Health [http://rsbweb.nih.gov/ij/index.html]). The rate of PEA15 protein degradation was plotted after normalizing the band intensity of PEA15 protein to that of the corresponding actin and expressing the values as a proportion of the initial levels of PEA15. Karyotyping of HCT116 cells was performed at the cytogenetics laboratory of Yale University School of Medicine. Metaphase-arrested chromosomes were visualized by Giemsa banding. Five individual metaphase spreads were analyzed to ensure homogeneity of karyotype (data not shown).

Chemical inhibitors. Lactacystin (Calbiochem) was added 8 h before whole-cell lysate preparation at the concentrations indicated in the figures. Etoposide was added at a concentration of 10 μM or 20 μM, and doxorubicin was added at a concentration of 0.1 μg/ml or 0.2 μg/ml for 24 h or for durations indicated in the figures. Cycloheximide (Sigma-Aldrich) was added at the final concentration of 50 μg/ml, immediately after gamma irradiation (20 Gy) or along with etoposide (10 μg/ml) or doxorubicin (0.1 μg/ml). ATM inhibitor (Calbiochem) was added to a final concentration of 10 μM at 30 min before irradiation. The neddylation inhibitor MLN-4924 (Millennium Pharmaceuticals) was added at the concentrations indicated in the figures (typically 0.5 and 1 μM) for a period of 24 h. For samples that were gamma irradiated, MLN-4924 was added 30 min before irradiation, and lysates were collected 24 h after gamma irradiation. Cells were treated with U0126 (Cell signaling) at a concentration of 10 μM for 24 h. For fluorescence-activated cell sorting (FACS) analysis following G_1 synchronization using a double thymidine block, U0126 was added immediately after the cells were released into fresh medium at a final concentration of 10 μM. For soft-agar assay, U0126 was added at a concentration of 10 μM, and cells were supplemented with fresh medium containing U0126 every 48 h for the duration of the soft-agar assay. *N*-Ethylmaleimide (NEM) (Sigma) was used at a concentration of 4 mM, and ubiquitin aldehyde (Santa Cruz) was used at a concentration of 0.5 μM for *in vitro* deubiquitination assays until the end of the reaction.

Cell cycle and mitotic index analyses. (i) FACS analysis to measure cell cycle stage-dependent expression of PEA15. Cells were synchronized by a double thymidine block as described previously (15). Arrested cells were then washed in 1× phosphate-buffered saline (PBS) and released by growth in Dulbecco's modified Eagle's medium (DMEM) with 10% fetal bovine serum (FBS). At time points indicated in the figure legends, cells were harvested and split into two parts: one part was lysed for immunoblot analysis, and the other was fixed with 85% ethanol and processed for cell cycle analysis by FACS. Cells were synchronized in G_2/M phase by nocodazole arrest as described previously (15). Cells were collected at the time points in the figure legends and processed as described above. Cells were stained with propidium iodide, and cell cycle distributions were determined by FACS analysis. Quantitation of the fraction of cells in different cell cycle phases was done using FlowJo software. The numbers of cells in G_1 (2n DNA), S phase (>2n and <4n DNA), and G_2/M (4n DNA) were quantified, and the percent fraction of cells in each phase was calculated. Doublets and cell aggregates were removed by plotting the pulse

area (FL2A) against pulse width (FL2W) and by gating for single-cell populations.

(ii) FACS analysis to monitor cell cycle progression. HCT116 cells stably expressing nonsilencing (NS) and PEA15 shRNAs or PEA15 and CDK6 shRNAs were synchronized by double thymidine block. Arrested cells were then washed with 1× PBS and released by culturing them in DMEM with 10% FBS with or without U0126 (10 μM). Cells were collected at 0, 4, and 10 h after release from s double thymidine block and processed for cell cycle analysis by FACS analyses. Linear histograms for intensity of staining in the FL2 channel (FL2A) were captured using a BD FACSCalibur instrument (BD Biosciences). Quantitation of the fraction of cells in different cell cycle phases was done using FlowJo software. The numbers of cells in G_1 (2n DNA), S phase (>2n and <4n DNA), and G_2/M (4n DNA) were quantified, and the percent fraction of cells in each phase was calculated. Doublets and cell aggregates were removed by plotting FL2A against FL2W and by gating for single-cell populations.

(iii) FACS analysis to measure G_2/M checkpoint defect. For cell cycle analysis after gamma irradiation, HCT116 cells stably expressing control or *PEA15* shRNAs were seeded at 2×10^5 cells/well in six-well plates and exposed to 20 Gy of ionizing radiation. Cells were collected at various time points after irradiation as indicated in the figures, fixed with 85% ethanol, stained with propidium iodide, and analyzed by FACS as described previously (14). Linear histograms for intensity of staining in the FL2 channel (FL2A) were captured using a BD FACSCalibur instrument (BD Biosciences). Quantitation of the fraction of cells in different cell cycle phases was done using FlowJo software. The numbers of cells in G_1 (2n DNA), S phase (>2n and <4n DNA), and G_2/M (4n DNA) were quantified, and percent fraction of cells in each phase was calculated. Doublets and cell aggregates were removed by plotting FL2A against FL2W and by gating for single-cell populations.

(iv) Mitotic index. The mitotic index was measured as described previously (16). Briefly, HCT116 cells carrying an NS or PEA15 shRNA were subjected to 5 Gy of gamma irradiation. Nocodazole was added 1 h after irradiation for a period of 16 h. Cells were fixed and stained for phospho-Ser10 histone H3 (Millipore).

Clonogenic assay and spontaneous mutagenesis assay. The clonogenic ability of the HCT116 cells stably expressing a control or *PEA15* shRNA was measured under unirradiated and gamma-irradiated conditions. For clonogenic assay, 2×10^5 cells were seeded in a six-well plate, and 48 h after a 2-Gy dose of gamma irradiation 5×10^3 cells were reseeded in another six-well plate. As an unirradiated control, 5×10^3 cells were seeded in a six-well plate. After 6 to 8 days of plating, colonies were fixed with a fixing solution containing 50% methanol and 10% acetic acid and then stained with 0.05% crystal violet (Sigma-Aldrich). The relative number of colonies was calculated by normalizing the average colony number of the triplicates carrying indicated shRNAs against those carrying NS shRNA. The spontaneous mutagenesis assays were performed as described previously (17). Briefly, HCT116 cells stably expressing a control or *PEA15* shRNA were seeded at 5×10^3 cells/well in a 48-well plate. 6-Thioguanine (5 μg/ml; Sigma-Aldrich) was added to the cells, and cells were grown for 2 weeks. The surviving colonies were fixed using solution containing 50% methanol and 10% acetic acid and then stained with 0.05% crystal violet (Sigma-Aldrich). The assay was carried out in triplicates, and the mutation rate was calculated as the ratio of the number of 6-thioguanine-resistant colonies to the total number of cells seeded in a 48-well plate and is expressed as $n \times 10^{-5}$.

Co-IP, polyubiquitination analyses, and phospho-SQ immunoprecipitation. Coimmunoprecipitation (co-IP) analyses were performed as described previously (14). For analyzing the interaction of endogenous PEA15 and COPS5, PEA15 was immunoprecipitated using anti-PEA15 antibody from HCT116 whole-cell lysate, and the immunoprecipitate was analyzed for COPS5 through immunoblotting with anti-COPS5 antibody. For analyzing the interaction of PEA15 with wild-type COPS5 (COPS5-WT) and COPS5-S320A under nonirradiated and gamma-irradiated conditions, HCT116 cells were transfected with GFP-PEA15 along with a MYC–COPS5-WT or MYC–COPS5-S320A plasmid and left unirradiated or gamma irradiated. GFP-PEA15 was immunoprecipitated with anti-GFP antibody, and the immunoprecipitate was analyzed for MYC-COPS5 through immunoblotting with anti-MYC antibody. For PEA15 ubiquitination analysis, HCT116 cells expressing control or *COPS5* shRNAs were transfected with GFP-PEA15 and hemagglutinin (HA)-ubiquitin mammalian expression vectors. Cells were exposed to 20 Gy of gamma radiation, cultured for 24 h, and then lysed. Ubiquitinated proteins were immunoprecipitated using anti-HA antibody (Sigma), and polyubiquitinated PEA15 protein was detected by immunoblotting using anti-GFP antibody (Santa Cruz) for detecting the GFP-PEA15 fusion protein. For COPS5 ubiquitination analysis, HCT116 cells were transfected with COPS5 and HA-ubiquitin expression vectors. Cells were treated with or without ATM kinase inhibitor (Calbiochem) at a final concentration of 10 μM and gamma irradiated (20 Gy) or left unirradiated. Cells were lysed after 24 h, and ubiquitinated proteins were immunoprecipitated using anti-HA antibody (Sigma-Aldrich). Polyubiquitinated COPS5 protein was detected by immunoblot analysis by using COPS5 antibody (Santa Cruz). For phospho-SQ immunoprecipitation, HCT116 cells with and without ATM kinase inhibitors (10 μM) were irradiated with 20 Gy of gamma irradiation or left unirradiated. At 24 h after gamma irradiation, cells were lysed, and potential ATM target proteins were immunoprecipitated using phospho-SQ antibody. The precipitated proteins were separated by SDS-PAGE and analyzed for COPS5 by immunoblot analyses.

***In vitro* deubiquitination assay for polyubiquitinated PEA15.** *In vitro* deubiquitination assays were carried out using immunoprecipitated COPS5, COPS5-D151N, or GST-COPS5 and GST–COPS5-D151N purified from *Escherichia coli*. HCT116 cells were transfected with MYC-COPS5-pCDNA3.1 or MYC–COPS5-D151N–pCDNA3.1 or the vector, followed by immunoprecipitation of the tagged proteins using anti-MYC antibody (Santa Cruz) and immobilization with protein G beads. The *in vitro* deubiquitination assays were performed similarly to a previously described method with minor modifications (18). The reaction mixtures were resolved on a 6% SDS-PAGE gel and probed with anti-HA antibody to detect the ubiquitinated fraction of GFP-PEA15 protein. For GST purification, COPS5 and COPS5-D151N were cloned in pGEX4-1T. Purification of all GST-tagged proteins and GST was done as described previously (16). Briefly, GST-tagged proteins cloned in bacterial expression constructs were transformed into the BL21 pLyse strain of *E. coli*. After 3 h of induction with 0.1 mM isopropyl-β-D-thiogalactopyranoside (IPTG; Sigma-Aldrich), bacterial pellets were lysed by sonication and incubated overnight with glutathione-agarose beads (Pierce). The GST-tagged proteins bound to the agarose beads were eluted with 10 mM reduced glutathione (Sigma-Aldrich).

Kinase assays. CDK6 and CDK1 kinase assays were performed as described previously (19). Briefly, CDK6 and CDK1 complexes were immunoprecipitated from HCT116 cells stably expressing either NS or PEA15 shRNA. A kinase reaction was set in 10× assay buffer (100 mM magnesium acetate, 200 mM dATP, 10 mM dithiothreitol [DTT]), 10 μCi of [γ-^{32}P]dATP (Perkin-Elmer), and 2 μg of substrate per reaction. For CDK6, purified GST-pRB (where RB is retinoblastoma) was used as the substrate and for CDK1; histone H1 (Millipore) was used as the substrate for CDK1. The reaction was terminated by the addition of 30 μl of 2× Laemmli sample buffer and boiled for 5 min. Samples were fractionated on a 12% polyacrylamide gel. The gel was dried and analyzed by autoradiography. The cell lysates were resolved by running SDS-PAGE, and proteins were transferred to polyvinylidene difluoride (PVDF) membranes, which were probed using anti-CDK6, anti-CDK1, and anti-cyclin B antibodies. For an ATM kinase assay, full-length wild-type COPS5 and phosphorylation site mutants T154A and S320A cloned as GST fusion proteins were expressed and purified from *E. coli*. An *in vitro* ATM kinase assay was performed as described previously (20). HCT116 cells were transfected with plasmids expressing FLAG-tagged ATM or the kinase-dead (KD) mutant form (ATM-KD). ATM was immunoprecipitated with anti-FLAG M2 beads (Sigma) and incubated with 10 μCi of [γ-^{32}P]ATP

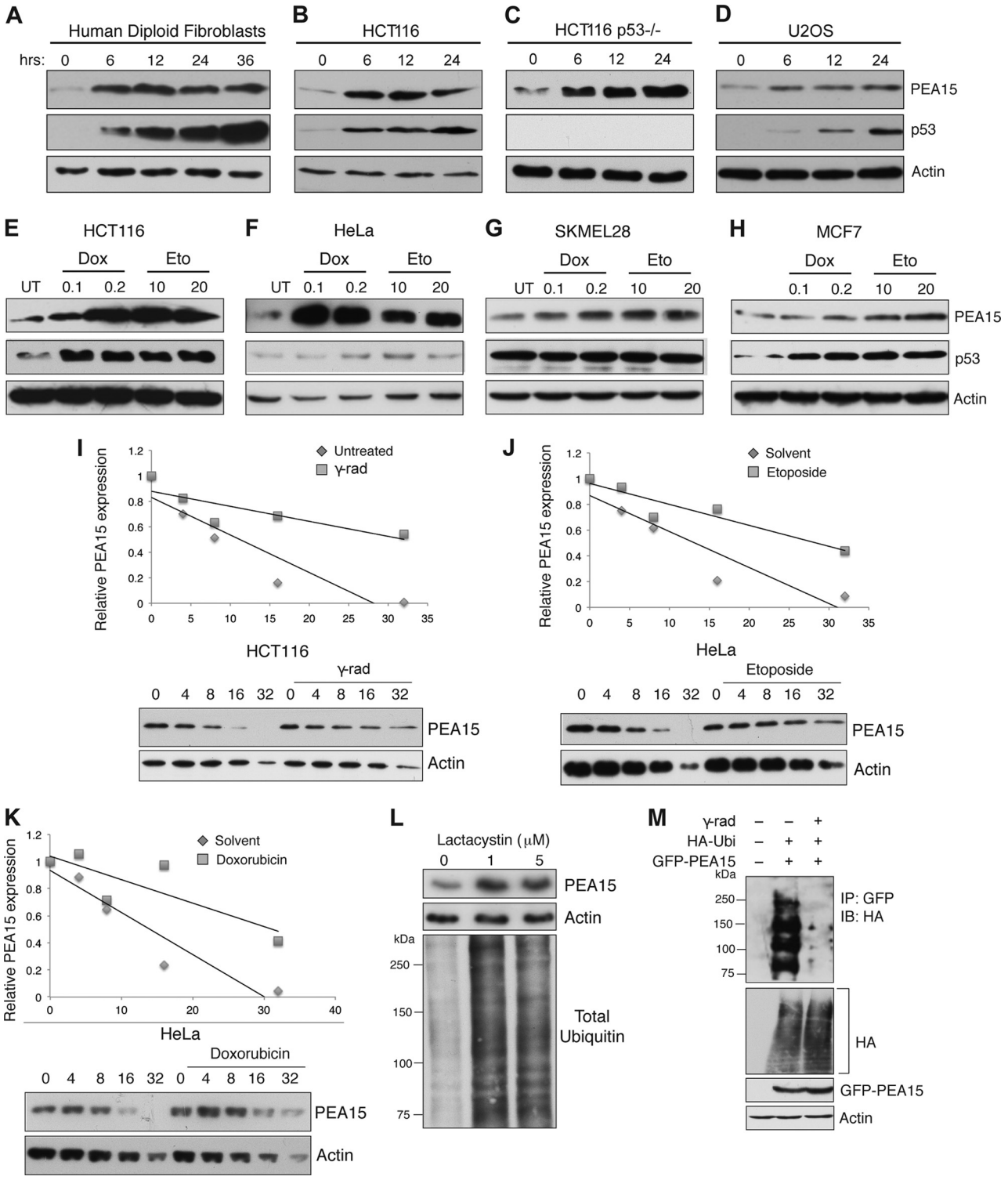

FIG 1 PEA15 protein is stabilized after DNA damage. (A to D) Immunoblot analysis of PEA15 and p53 at indicated time points following 20-Gy gamma irradiation in human diploid fibroblasts, HCT116 cells, HCT116 $p53^{-/-}$ cells, and U2OS cells. Actin was used as the loading control. (E to H) Immunoblot analysis of PEA15 and p53 after 24 h following treatment with 0.1 or 0.2 μg/ml doxorubicin (Dox) and 10 or 20 μM etoposide (Eto) in HCT116, HeLa, SKMEL-28, and MCF7 cells. Actin was used as the loading control. (I) A cycloheximide chase experiment was performed in HCT116 cells. Relative PEA15 levels in cells treated with cycloheximide (50 μg/ml) without or with gamma irradiation (γ-rad) at indicated time points were normalized to actin and plotted. (J and K) A cycloheximide chase experiment was performed in HeLa cells. Relative PEA15 levels in cells treated with cycloheximide (50 μg/ml) without or with etoposide (J) or doxorubicin (K) treatment at indicated time points were normalized to actin and plotted. (L) Immunoblot analysis for the indicated proteins treated with increasing concentrations of lactacystin. (M) Immunoblot (IB) analysis to monitor polyubiquitination of PEA15 protein in gamma-irradiated HCT116 cells. Additional indicated proteins were analyzed as internal controls. UT, untreated; Ubi, ubiquitin.

and 1 μg of GST fusion substrates for 20 min at 30°C. The reaction was stopped by the addition of SDS-PAGE protein sample buffer, and proteins were separated by SDS-PAGE and detected by autoradiography.

Soft-agar assay and tumorigenesis assay. Soft-agar assays were performed by plating 5×10^3 MEF/SV40-ER or MEL-ST cells stably expressing various constructs, as indicated in the figures, into 0.35% low-temperature-gelling agarose (Sigma-Aldrich) and layered on top of a 0.7% agarose base. After 4 weeks of growth, colonies were stained with 0.005% crystal violet solution. MEF/SV40-ER cells (0.5×10^6) expressing HRAS v12 alone, HRAS v12 and PEA15, or HRAS v12, PEA15, and CDK6 were injected subcutaneously into athymic nude (NCr nu/nu) mice (8 weeks old). Tumor volumes were calculated using the following formula: length × width^2 × 0.5. All animal experiments were approved by the Institutional Animal Care and Use Committee (IACUC) at Yale University and were performed in accordance with the IACUC guidelines.

Global protein-protein interaction screening by using the yeast two-hybrid method. A yeast two-hybrid screen was performed using the Matchmaker Gold Yeast Two-Hybrid System (Clontech) according to the manufacturer's protocol. The *PEA15* cDNA was cloned into pGBKT7 between NdeI and BamHI and in frame with the GAL4 DNA-binding domain (Gal4-DBD) and used as the bait. A normalized HeLa cell cDNA library in pGAD7 expressed as fusions to the GAL4 activation domain (Gal4-AD) was used as the prey. Candidate interactors were selected based on the activation of *HIS3*, *MEL1*, and *AUR1-C* reporter genes as blue (*MEL1*$^+$) aureobasidin A (AbaA)-resistant (*AUR1-C*$^+$) colonies that grow on triple-dropout medium (lacking leucine, tryptophan, and histidine) containing the chromogenic substrate X-alpha-Gal (Clontech) and the antifungal AbaA (Clontech). Candidate interactors identified by sequencing were validated by cloning individual cDNAs into the pGAD7 vector, introducing the vector into the two-hybrid selection strain, and mating it to a selection strain of the opposite mating type carrying the PEA15-Gal4-DBD bait. Positive interactions were detected after mating by growth on triple-dropout medium (lacking leucine, tryptophan, and histidine).

Microarray and data analyses. RNA was isolated from HCT116 cells stably expressing control or *PEA15* shRNAs and used to generate labeled antisense RNA using an Ambion MessageAmp Kit and hybridized to the Illumina Human HT-12, version 3.0, expression bead chip using Illumina's protocol. Array signals processed using GenomeStudio (Illumina) were $\log_2$ transformed and quantile normalized using the lumi package in Bioconductor (21). Sample quality control (QC) was performed according to the manufacturer's protocol and included various control plots and other general microarray analysis-related methods; all the samples passed QC (data not shown). Differential expression analysis was performed using the Limma package. A moderated *t* test (22) and Benjamini-Hochberg multiple test correction procedure (23) were used to identify statistically significant changes in gene expression (adjusted *P* value, <0.05). MetaCore (version 6.8, build 29806; GeneGo Inc.) was used to identify significantly enriched pathways based on differentially expressed genes.

Colon cancer, lung cancer, and breast cancer samples and bisulfite sequencing and Me-DIP assay. Total RNAs from normal, colorectal cancer, breast cancer, and lung cancer samples were obtained from the University of Massachusetts Medical School (UMMS) Tissue and Tumor Bank. Genomic DNA was extracted from cryopreserved patient samples obtained from the UMMS Tissue and Tumor Bank. Bisulfite sequencing was performed as described previously (9). The following primers were used for PEA15 bisulfite sequencing: forward, 5′-GAGTTTTTTAGAATTTTAGTTTTT-3′; reverse, 5′-TACCCCTCCAAACCTAAAC-3′; forward, 5′-TTGTTTTTTTATTTTTTTTTTTTTTTT-3′; reverse, 5′-TAAAACCTAACACAAAATAAACT-3′. A methyl-DNA immunoprecipitation (Me-DIP) assay was performed as described previously (24). Genomic DNA extracted from normal and cancerous tissues was subjected to sonication to obtain 300- to 100-bp fragments. The DNA was denatured for 10 min at 95°C and immunoprecipitated for 2 h at 4°C with 10 μl of monoclonal antibody against 5-methylcytidine (Eurogentec) in a final volume of 500 μl of IP buffer (10 mM sodium phosphate [pH 7.0], 140 mM NaCl, 0.05% Triton X-100). The antibody-bound DNA was isolated using 30 μl of Dynabeads. Methylated DNA was recovered by proteinase K treatment, followed by phenol-chloroform extraction and ethanol precipitation. The following primers were used for Me-DIP analyses: PEA15 Me-DIP forward, 5′-AGTCTTCCAGAACCCCCAGC-3′; reverse, 5′-AGTCCCCGGTTCCTAAGCAG-3′.

Microarray data accession number. *PEA15* expression data have been deposited in the Gene Expression Omnibus (GEO) under accession number GSE39297.

TABLE 1 List of PEA15-interacting proteins identified by yeast two-hybrid screening[a]

Gene symbol	Accession no.	Name
ATP1B3	NM_001679.2	ATPase, Na/K transporting, beta 3 peptide
C5orf44	NM_001093755	Chromosome 5 open reading frame 44
CACYBP/SIP	NM_014412.2	Calcyclin binding protein
CEP120	NM_153223.2	Centrosomal protein 120 kDa
COPS5	**NM_006837**	**COP9 signalosome subunit 5**
DNAJB1	NM_006145	DnaJ (HSP40) homolog, subfamily B, member 1
DYRK1A	NM_130438.2	Dual-specificity tyrosine phosphorylation-regulated kinase 1A
FAM103A1	NM_031452.2	Family with sequence similarity 103, member A1
KLHL12	NM_021633.2	Kelch-like 12
MTIF3	NM_152912.4	Mitochondrial translation initiation factor 3
OSBPL1A	NM_018030.3	Oxysterol binding protein like 1A
PAPD5	NM_001040284.2	PAP associated domain containing 5
PDE4DIP	NM_014644	Phosphodiesterase 4D interacting protein isoform 3
PGM1	NM_002633.2	Phosphoglucomutase 1
PLD1	NM_001130081.1	Phospholipase D1, phosphatidylcholine specific
PUS3	NM_031307.3	Pseudouridylate synthase 3
RSL24D1	NM_016304.2	Ribosomal L24 domain containing 1
SNRPG	NM_003096.2	Small nuclear ribonucleoprotein polypeptide G
SMEK1	NM_032560.4	Suppressor of MEK1
SON	NM_138927	SON DNA binding protein
TALDO1	NM_006755.1	Transaldolase 1
TJP1	NM_175610.2	Tight junction protein 1

[a] All proteins were identified by yeast two-hybrid screening. In addition, the product of *COPS5* (in boldface) was identified by coimmunoprecipitation.

RESULTS

DNA damage stabilizes PEA15 through a posttranslational mechanism. DNA damage has been shown to provide a signal that activates tumor suppressors, which in turn induce cellular senescence (4, 5). We therefore monitored the expression of PEA15 in a variety of human cell lines after inducing DNA damage with gamma radiation or chemotherapeutic agents. We found that PEA15 protein levels increased in response to DNA damage (Fig. 1A to H). The increase in PEA15 protein levels appears to be posttranslational as DNA damage did not increase *PEA15* mRNA levels (data not shown). Moreover, DNA damage increased PEA15 protein even in the presence of the translation inhibitor cycloheximide (data not shown), and cycloheximide chase experiments revealed that DNA damage increased the half-life of PEA15 protein (Fig. 1I to K). These findings suggest that DNA damage increases PEA15 protein stability.

DNA damage stabilizes some tumor suppressor proteins, such as p53, via posttranslational mechanisms that prevent their proteasome-mediated degradation (25). We therefore asked whether PEA15 stability is similarly regulated by proteasome-mediated degradation. Indeed, treatment of HCT116 cells with the protea-

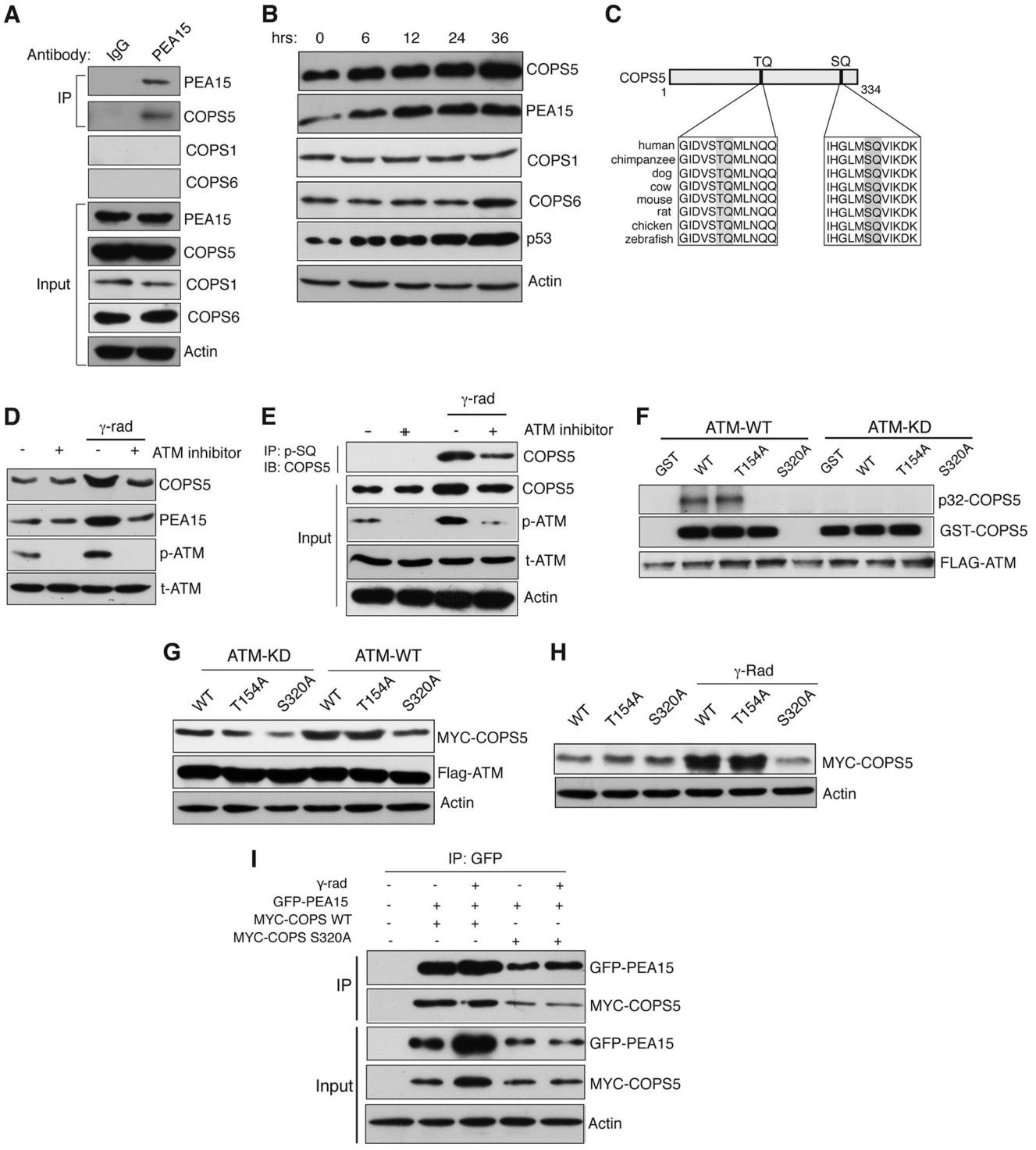

FIG 2 PEA15 protein stability is regulated by the proteasomal degradation pathway. (A) Immunoblot analysis for indicated proteins after immunoprecipitation (IP) with IgG control or PEA15 antibody. Input was also analyzed for the indicated proteins. (B) Immunoblot analysis of the indicated proteins at the indicated time points after gamma irradiation. Actin was used as a loading control. (C) Schematic indicating two evolutionarily conserved potential ATM kinase phosphorylation sites. (D) Immunoblot analysis for the indicated proteins before and after gamma irradiation with or without treatment with the ATM inhibitor (10 μM). (E) Immunoblot analysis of COPS5 after immunoprecipitation of the phospho-SQ fraction of HCT116 cells isolated under the indicated conditions. As controls, the indicated proteins were analyzed in the input. (F) Autoradiograph of ^{32}P-labeled GST–COPS5-WT, GST–COPS5-T154A, and GST–COPS5-S320A after incubation with ATM or ATM-KD. Immunoblots of GST-COPS5 substrates and FLAG-ATM are also shown. (G) Immunoblot analysis of the indicated proteins in HCT116 cells expressing COPS5 WT, T154A, and S320A proteins along with ATM-FLAG KD or ATM-FLAG WT plasmids. (H) Immunoblot analysis of MYC-COPS5 and actin in HCT116 cells ectopically expressing COPS5 WT, T154A, or S320A proteins left untreated or irradiated with 20-Gy gamma radiation. (I) Immunoblot analysis after immunoprecipitation (IP) with PEA15 antibody in HCT116 cells that were unirradiated or gamma irradiated. The indicated proteins were analyzed in the inputs as controls.

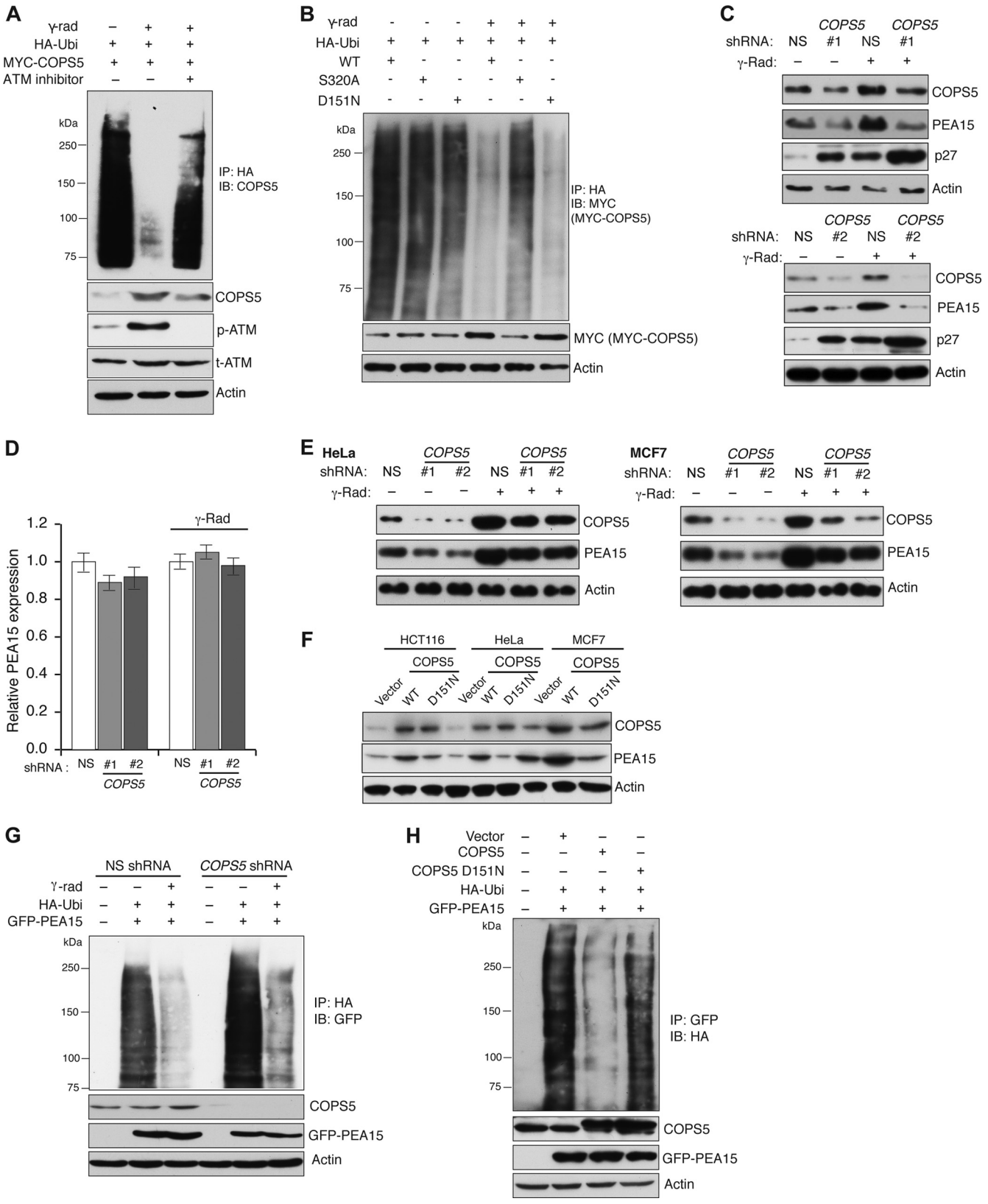

FIG 3 COPS5 is stabilized by ATM-mediated phosphorylation. (A) Immunoblot analysis of COPS5 from immunoprecipitates of polyubiquitinated (HA) proteins. Lysates from cells expressing HA-tagged ubiquitin (HA-Ubi) and COPS5 under the unirradiated or gamma-irradiated condition or under the condition of gamma irradiation with ATM kinase inhibitor treatment. Immunoblots of COPS5 and actin are also shown. (B) Immunoblot analysis of MYC-COPS5 from immunoprecipitate of polyubiquitinated (HA) proteins. Lysates from cells expressing HA-tagged ubiquitin (HA-Ubi) and MYC–COPS5-WT, MYC–COPS5-

some inhibitor lactacystin stabilized PEA15 (Fig. 1L). Strikingly, we found that polyubiquitination of PEA15 was drastically reduced following gamma irradiation (Fig. 1M). These results indicate that DNA damage stabilizes PEA15 by preventing polyubiquitination and turnover by proteasome-mediated degradation.

COPS5 stabilizes PEA15 by deubiquitination in an ATM kinase-dependent manner. To identify factors that may directly regulate PEA15 ubiquitination and thus stability, we performed a large-scale yeast two-hybrid screen (Table 1). One of the PEA15-interacting proteins identified by this screen was the COP9 signalosome (CSN) subunit COPS5, a JAMM (JAB1/MPN/Mov34 metalloenzyme) motif protein with deubiquitinase (DUB) activity (26). Interestingly, COPS5-mediated deubiquitination was previously shown to stabilize target proteins (27). Furthermore, COPS5 is implicated in DNA repair, cell cycle progression, and tumorigenesis (28), making it a high-priority PEA15-interacting protein for follow-up studies. We confirmed via coimmunoprecipitation that endogenous PEA15 and COPS5 interact in HCT116 cells (Fig. 2A) and found that, similar to PEA15, COPS5 expression increases in response to DNA damage (Fig. 2B). Notably, COPS5 interacted with PEA15 independent of its ability to interact with other components of the COP9 signalosome (CSN) complex, such as COPS1 and COPS6 (Fig. 2A).

To determine the mechanism of COPS5 stabilization following DNA damage, we analyzed the COPS5 protein sequence and identified two evolutionarily conserved potential ATM kinase phosphorylation sites (TQ and SQ) (Fig. 2C) (29). Importantly, pharmacological inhibition of ATM kinase prevented DNA damage-induced COPS5 stabilization (Fig. 2D). Notably, following gamma irradiation, SQ site phosphorylation of COPS5 increased, which was blocked by treatment with an ATM inhibitor (Fig. 2E). To identify the amino acid residue of COPS5 that is phosphorylated by ATM, we generated two site-directed mutants of COPS5 that lacked one of the two predicted ATM phosphorylation sites and performed an *in vitro* kinase assay using either the wild-type ATM kinase (ATM-WT) or, as a control, the kinase-dead ATM (ATM-KD). Consistent with the results shown in Fig. 2E, Fig. 2F shows that ATM phosphorylates COPS5 at serine 320. Moreover, the COPS5-S320A mutant, which cannot be phosphorylated by ATM, was not stabilized by ectopic expression of ATM or following irradiation (Fig. 2G and H). The PEA15-COPS5 interaction was not dependent upon DNA damage or ATM-mediated phosphorylation of COPS5 at serine 320 (Fig. 2I).

Finally, to understand why ATM-mediated phosphorylation stabilizes COPS5, we measured COPS5 polyubiquitination before and after gamma irradiation. Figure 3A shows that gamma irradiation led to significant reduction in COPS5 polyubiquitination, which was increased by an ATM inhibitor. Furthermore, ATM-mediated phosphorylation of COPS5 at S320 was required for preventing COSP5 polyubiquitination after gamma irradiation (Fig. 3B). However, ectopic expression of a COPS5 JAMM domain mutant (D151N) that lacks deubiquitinase activity (30), similar to wild-type COPS5, underwent increased deubiquitination (Fig. 3B). Collectively, these results show that following DNA damage, ATM phosphorylates COPS5 at Ser320, which prevents its polyubiquitination and consequentially stabilizes COPS5 following gamma irradiation. However, COPS5 stabilization is not dependent upon its deubiquitinase activity.

We next tested whether COPS5 promotes PEA15 stability after DNA damage. Toward this end, we used shRNAs to knock down *COPS5* expression and monitored PEA15 protein levels following irradiation. Notably, *COPS5* knockdown prevented PEA15 stabilization after DNA damage without affecting PEA15 mRNA levels (Fig. 3C and D). Similar to the results in HCT116 cells, knockdown of *COPS5* inhibited expression of PEA15 (Fig. 3E), and ectopic expression of COPS5 was sufficient to stabilize PEA15 in a variety of cancer cell lines (Fig. 3F). In cells lacking COPS5, the reduced PEA15 protein levels correlated with increased polyubiquitination of PEA15 (Fig. 3G). Conversely, ectopic expression of COPS5 reduced PEA15 polyubiquitination and increased PEA15 levels (Fig. 3H). Ectopic expression of COPS5-D151N that lacks deubiquitinase activity (30) failed to efficiently deubiquitinate PEA15 (Fig. 3H).

Previous studies have shown that COPS5 is a subunit of the eight-subunit CSN complex (31–33). Among many described biological activities, the CSN complex has been shown to function as a Cullin 1 (CUL1) deneddylating enzyme, and purified CSN can cleave NEDD8 from CUL1 (34). Moreover, CUL11 neddylation enhances the ability of SCF to ubiquitinate proteins (31). Therefore, we first asked whether knockdown of COPS5 inhibits PEA15 protein stability by regulating CUL1 neddylation. To do so, we treated cells with the neddylation inhibitor MLN-4924 and monitored PEA15 levels following gamma irradiation. Figure 4A shows that MLN-4924 did not prevent PEA15 stabilization following gamma irradiation. In further support of the role of COPS5 in regulating PEA15 stability, shRNA-mediated knockdown of other components of the CSN complex (*COPS1*, *COPS3*, and *COPS6*) or *USP15*, a deubiquitinase that has been previously shown to associate with the CSN complex (27), did not affect PEA15 stabilization (Fig. 4B and C).

Next, we tested the ability of COPS5 to deubiquitinate PEA15 *in vitro*. Consistent with its possible role as a deubiquitinase, COPS5 purified from mammalian cells deubiquitinated PEA15 (Fig. 4D), whereas purified COPS5-D151N protein failed to do so (Fig. 4E). To rule out the association of contaminating deubiquitinase (DUB) activity with COPS5 and the role of other CSN subunits in PEA15 stabilization, we purified COPS5 and COPS5-D151N as GST fusion proteins from bacteria and tested their

S320A, and MYC–COPS5-D151N without or with gamma irradiation were used. Immunoblots of COPS5 and actin are also shown. (C) Immunoblot analysis for COPS5, PEA15, and p27 proteins in gamma-irradiated HCT116 cells expressing NS or *COPS5* shRNAs (shRNA 1 and shRNA 2). Actin was used as a loading control. (D) qRT-PCR analysis of *PEA15* mRNA ($n = 3$) in HCT116 cells carrying NS or *COPS5* shRNAs without or with gamma irradiation. Error bars indicate standard errors of the means. (E) Immunoblot analysis of COPS5 and PEA15 levels in HeLa cells or MCF7 cells expressing NS or *COPS5* shRNAs without or with gamma irradiation. Actin was used as a loading control. (F) Immunoblot analysis of PEA15 and COPS5 in HCT116, HeLa, and MCF7 cells expressing vector control, COPS5-WT, and COPS5-D151N. Actin was used as a loading control. (G) Immunoblot analysis of PEA15 polyubiquitination (HA) after HA IP from unirradiated or gamma-irradiated cells expressing HA-tagged ubiquitin (HA-Ubi) and GFP-PEA15 in the presence of a nonsilencing (NS) control or *COPS5* shRNA. As controls immunoblots for the indicated proteins are shown. (H) Immunoblot analysis of PEA15 polyubiquitination (HA) after GFP-PEA15 immunoprecipitation from cells expressing a vector control or wild-type or mutant (D151N) COPS5 cDNA. The levels of COPS5, GFP-PEA15, and actin are shown as controls.

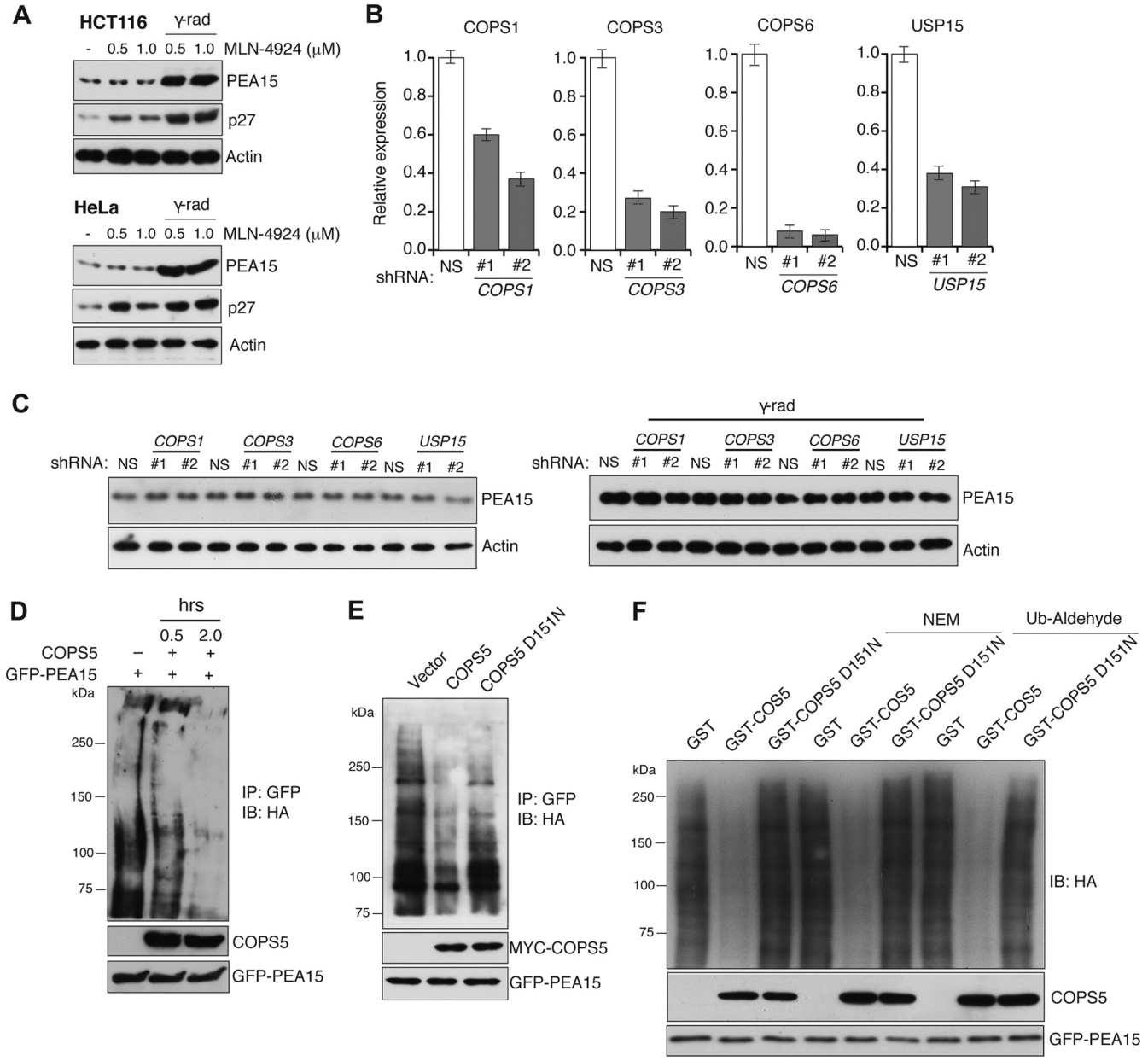

FIG 4 COPS5 stabilizes PEA15 protein by deubiquitination. (A) Immunoblot of PEA15 and p27 in HCT116 or HeLa cells treated with indicated concentrations of MLN-4924 under unirradiated or gamma-irradiated conditions. Actin is used as the loading control. (B) RT-qPCR analysis to measure mRNA levels ($n = 3$) of *COPS1*, *COPS3*, *COPS6*, and *USP15* in HCT116 cells stably expressing an NS shRNA or two different shRNAs (1 and 2) against each of the indicated genes. Error bars indicate standard errors of the means. (C) Immunoblot analysis of PEA15 in HCT116 cells carrying the indicated shRNAs under unirradiated (left) or gamma-irradiated (γ-rad) conditions (right). Actin is used as the loading control. (D) Immunoblot analysis of polyubiquitinated PEA15 probed with the antibody against HA incubated without or with immunoprecipitated COPS5 for the indicated time. (E) Immunoblot analysis of polyubiquitinated PEA15 probed with the antibody against HA incubated without or with immunoprecipitated COPS5 or COPS5-D151N for 30 min. (F) Immunoblot analysis of polyubiquitinated PEA15 probed with the antibody against HA that was incubated with purified GST or GST–COPS5-WT or GST–COPS5-D151N for 2 h in the absence or presence of NEM or ubiquitin (Ub) aldehyde.

ability to deubiquitinate PEA15 *in vitro*. In complete agreement with our other results, bacterially purified GST-COPS5 was able to deubiquitinate PEA15 *in vitro*, whereas the GST–COPS-D151N mutant failed to do so (Fig. 4F). Furthermore, GST-COPS5 was also able to deubiquitinate the polyubiquitinated PEA15 even in the presence of the cysteine-dependent DUB inhibitors *N*-ethylmaleimide (NEM) and ubiquitin aldehyde, ruling out any contaminating cysteine-dependent DUBs in our *in vitro* deubiquitination assay (Fig. 4F). Furthermore, knockdown of *USP15* did not affect PEA15 stability following DNA damage (Fig. 4C). Collectively, these results demonstrate that COPS5 deubiquitinates and stabilizes PEA15 following DNA damage.

Loss of PEA15 results in a DNA damage-induced G_2/M checkpoint defect due to increased CDC25C activity. DNA damage checkpoints couple cell cycle arrest to DNA repair (35). In many cases, proteins that are elevated in response to DNA damage

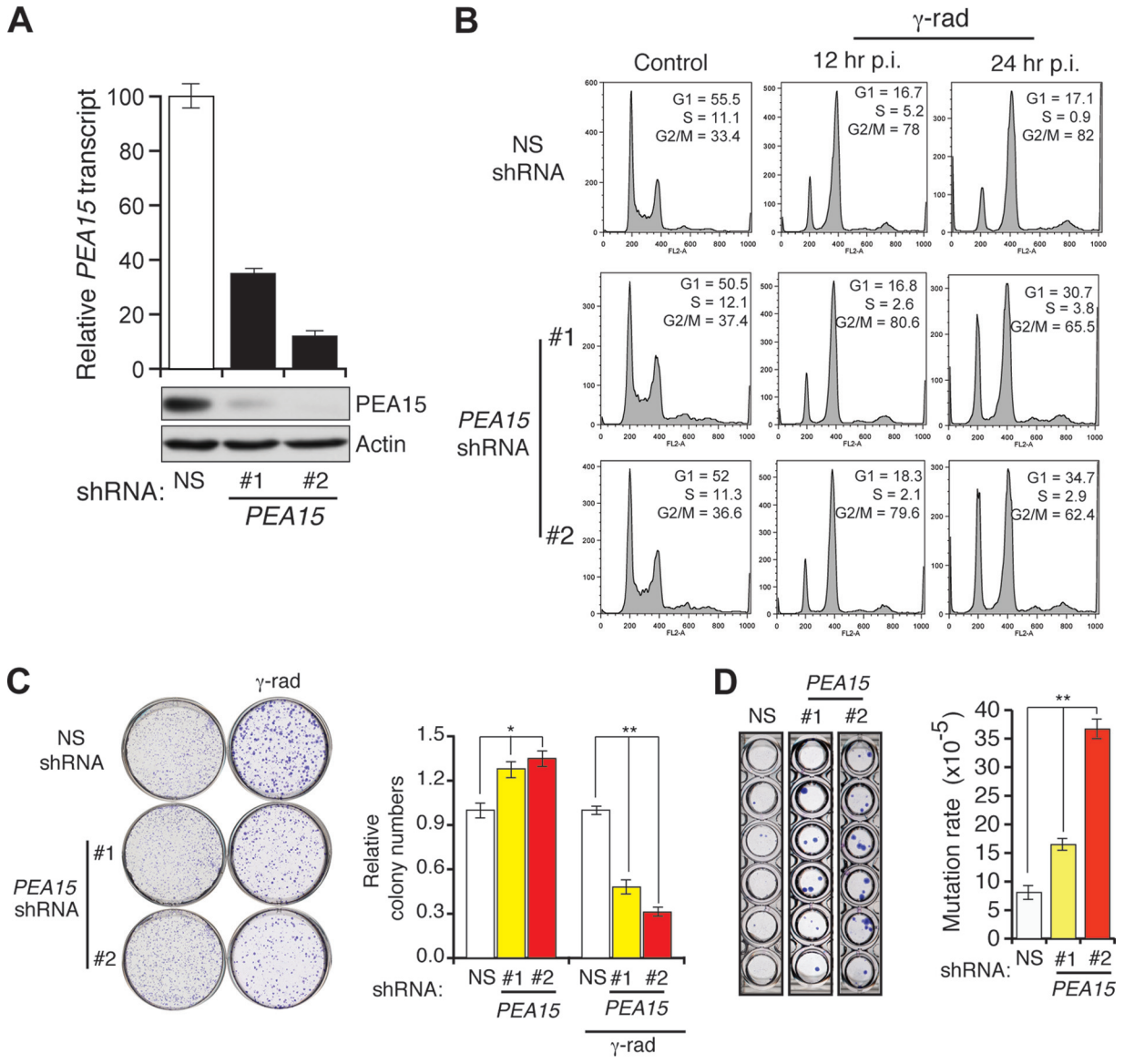

FIG 5 Loss of PEA15 causes DNA damage-induced G_2/M checkpoint defect and increased mutagenesis. (A) RT-qPCR analysis of *PEA15* mRNA levels ($n = 3$) (top) and immunoblot analysis of PEA15 levels (bottom) in HCT116 cells expressing NS or *PEA15* shRNAs (1 and 2). Actin was used as a loading control. Error bars indicate standard errors of the means. (B) Flow cytometry analysis to determine the cell cycle distribution of unirradiated (control) or gamma-irradiated HCT116 cells expressing the indicated shRNAs. Gamma-irradiated cells were collected at 12 or 24 h after irradiation. The percentage of cells in each stage of the cell cycle is indicated. (C) Clonogenic assay to monitor the survival of unirradiated and gamma irradiated (γ-rad) HCT116 cells expressing the indicated shRNAs ($n = 3$). Quantification of relative colony numbers is presented. Error bars indicate standard errors of the means. *, $P < 0.01$; **, $P < 0.001$. (D) Spontaneous mutation of the *hprt* gene ($n = 3$). Quantification of the mutation rate under the indicated conditions. Error bars indicate standard errors of the means. **, $P < 0.001$. Representative wells of crystal violet stained HCT116 cells expressing indicated shRNA that were grown in 6-TG are shown on the left.

function to regulate cell cycle checkpoints (35). We therefore asked whether loss of PEA15 compromises DNA damage-induced checkpoints by irradiating HCT116 cells stably expressing a *PEA15* or control shRNA (Fig. 5A). Figure 5B shows that *PEA15* knockdown resulted in defective DNA damage-induced G_2/M arrest. Consistent with this checkpoint defect, cells lacking PEA15 formed fewer colonies after gamma irradiation in a clonogenic assay (Fig. 5C) and had an increased rate of spontaneous mutagenesis (Fig. 5D). These findings indicate that PEA15 is necessary for the DNA damage-induced G_2/M checkpoint.

A previous study has shown that PEA15 sequesters ERK in the cytoplasm and that loss of PEA15 leads to increased nuclear ERK (11). At mitosis, ERK1/2 interacts with CDC25C and phosphorylates threonine 48 (T48), and ERK inhibition prevents CDC25C activation and induction of mitosis (36). Therefore, we asked whether regulation of CDC25C by ERK has a role in the ability of PEA15 to promote the DNA damage-induced G_2/M checkpoint. Toward this end, we first analyzed ERK localization both after shRNA-mediated knockdown of *PEA15* and with or without DNA damage. As expected, ERK accumulated in the nuclei of cells lacking PEA15 or after DNA damage (Fig. 6A). Notably, *PEA15* knockdown increased phosphorylation of CDC25C on T48,

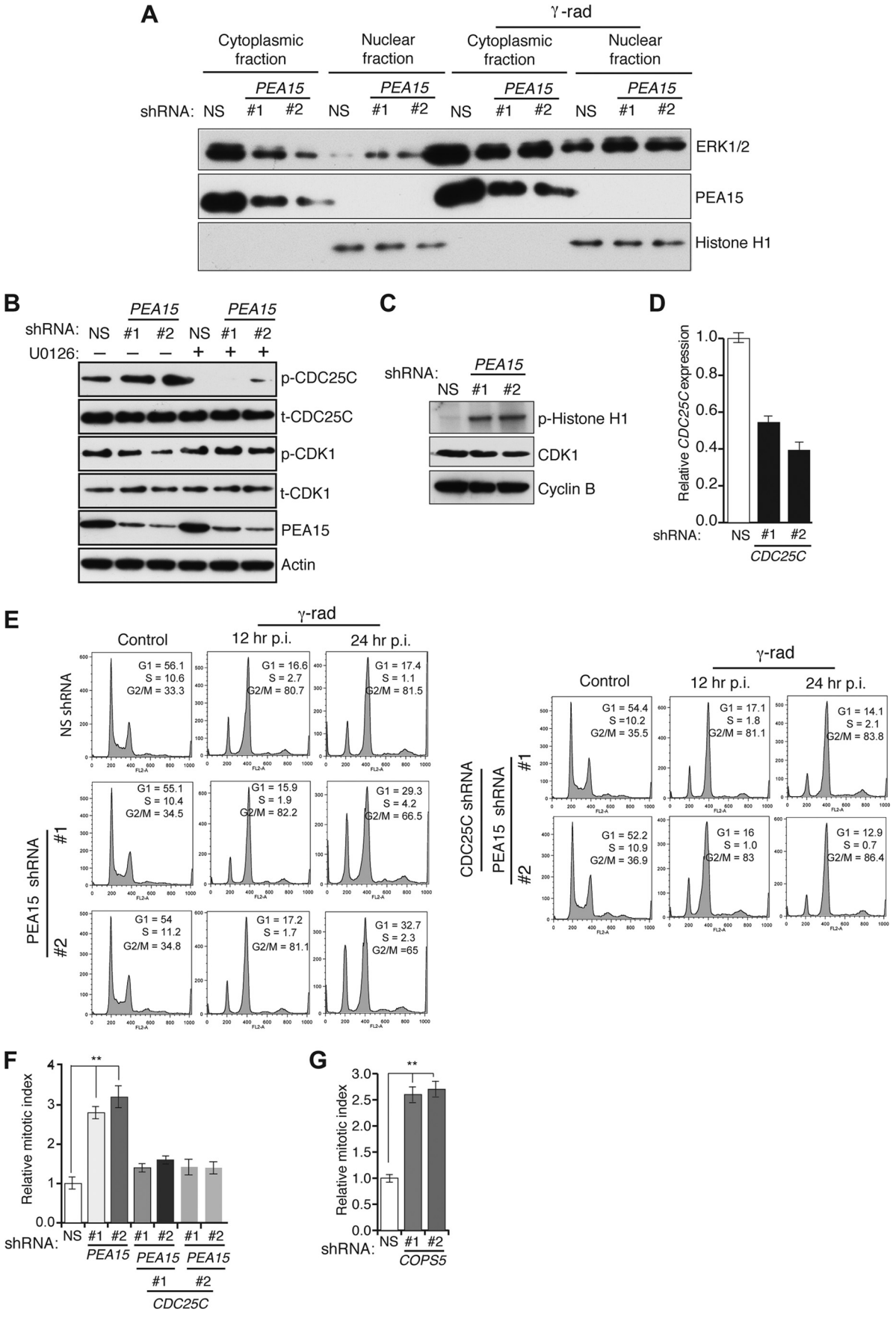
A
γ-rad
Cytoplasmic fraction
Nuclear fraction
Cytoplasmic fraction
Nuclear fraction
PEA15
shRNA: NS #1 #2 NS #1 #2 NS #1 #2 NS #1 #2
ERK1/2
PEA15
Histone H1
B
PEA15
shRNA: NS #1 #2 NS #1 #2
U0126: – – – + + +
p-CDC25C
t-CDC25C
p-CDK1
t-CDK1
PEA15
Actin
C
PEA15
shRNA: NS #1 #2
p-Histone H1
CDK1
Cyclin B
D
Relative CDC25C expression
1.0
0.8
0.6
0.4
0.2
0.0
shRNA: NS #1 #2
CDC25C
E
γ-rad
Control
12 hr p.i.
24 hr p.i.
NS shRNA
G1 = 56.1
S = 10.6
G2/M = 33.3
G1 = 16.6
S = 2.7
G2/M = 80.7
G1 = 17.4
S = 1.1
G2/M = 81.5
PEA15 shRNA #1
G1 = 55.1
S = 10.4
G2/M = 34.5
G1 = 15.9
S = 1.9
G2/M = 82.2
G1 = 29.3
S = 4.2
G2/M = 66.5
PEA15 shRNA #2
G1 = 54
S = 11.2
G2/M = 34.8
G1 = 17.2
S = 1.7
G2/M = 81.1
G1 = 32.7
S = 2.3
G2/M =65
γ-rad
Control
12 hr p.i.
24 hr p.i.
CDC25C shRNA
PEA15 shRNA #1
G1 = 54.4
S =10.2
G2/M = 35.5
G1 = 17.1
S = 1.8
G2/M = 81.1
G1 = 14.1
S = 2.1
G2/M = 83.8
PEA15 shRNA #2
G1 = 52.2
S = 10.9
G2/M = 36.9
G1 = 16
S = 1.0
G2/M = 83
G1 = 12.9
S = 0.7
G2/M = 86.4
F
Relative mitotic index
**
shRNA: NS #1 #2 #1 #2 #1 #2
PEA15
PEA15 PEA15
#1 #2
CDC25C
G
Relative mitotic index
**
shRNA: NS #1 #2
COPS5

which was blocked by treatment with the MEK inhibitor U0126 (Fig. 6B). CDC25C activity is required for the activation of CDK1/cyclin B activity (37, 38). We therefore tested whether loss of PEA15 increases CDK1/cyclin B activity, which in turn contributes to the DNA damage-induced G_2/M checkpoint defect. Figure 6C shows that CDK1/cyclin B activity is elevated in cells lacking PEA15. Simultaneous shRNA-mediated knockdown of CDC25C (Fig. 6D) and PEA15 restored the DNA damage-induced G_2/M checkpoint (Fig. 6E and F). Similar to the results with PEA15, knockdown of COPS5 led to an increase in CDC25C phosphorylation and the mitotic index, further supporting the role of COPS5 as an important regulator of PEA15 stability (Fig. 6G and 7I). Furthermore, the *COPS5* knockdown-mediated increase in CDC25C phosphorylation levels was reduced by U0126 treatment (Fig. 7I). Collectively, these results demonstrate that loss of PEA15 leads to ERK-mediated phosphorylation and activation of CDC25C, which in turn activates CDK1/cyclin B1, resulting in a DNA damage-induced G_2/M checkpoint defect.

Loss of PEA15 causes accelerated cell cycle progression by activating CDK6. We noticed that, even in the absence of DNA damage, HCT116 cells stably expressing PEA15 shRNA formed more colonies in liquid culture and had a shorter doubling time than control cells (Fig. 7A and B). These results suggested that PEA15 might also regulate normal cell cycle progression. Consistent with this idea, we found that PEA15 protein levels oscillate throughout the cell cycle, peaking early during G_2/M and declining rapidly before mitosis (Fig. 7C).

To understand how PEA15 controls proliferation, we performed a microarray analysis to identify genes with altered expression profiles in the absence of PEA15 and identified cyclin-dependent kinase CDK6 as a gene that is upregulated in the absence of PEA15 (Table 2 and Fig. 7D). Bioinformatics analysis of the CDK6 promoter predicted several binding sites for the c-JUN transcription factor. The data shown in Fig. 7E and F indicate that siRNA-mediated knockdown of c-*JUN* inhibited the transcriptional upregulation of CDK6 in cells depleted of PEA15. Thus, PEA15 negatively regulates c-JUN-dependent transcriptional activation of CDK6.

Nuclear ERK is required for c-JUN-mediated transcription (39). Because PEA15 binds to and sequesters ERK in the cytoplasm (11), we asked whether PEA15 regulates CDK6 expression through ERK. We treated cells expressing a PEA15 shRNA with the MEK inhibitor U0126 to prevent ERK activation. As predicted, inhibition of MEK prevented transcriptional upregulation of CDK6 in the absence of PEA15 (Fig. 7G). Finally, we used chromatin immunoprecipitation experiments to show that c-JUN directly binds to the CDK6 promoter. Association of c-JUN with the *CDK6* promoter increased following shRNA-mediated depletion of *PEA15*, which was prevented by treatment with the MEK inhibitor U0126 (Fig. 7H). Notably, consistent with COPS5 being a regulator of PEA15 stability, knockdown of COPS5 also resulted in increased expression of CDK6 (Fig. 7I). Collectively, these results indicate that PEA15 negatively regulates cell cycle progression by inhibiting the ERK-dependent, c-JUN-mediated transcriptional activation of *CDK6*.

Consistent with the increased CDK6 expression levels, we also observed elevated CDK6-associated kinase activity in cells expressing a PEA15 shRNA (Fig. 8A and B). To directly test whether PEA15 regulates cell cycle progression, we synchronized cells expressing a *PEA15* shRNA or a control shRNA by arresting them in G_1 using a double thymidine block or in G_2/M using nocodazole and then measured the fraction of cells in each phase of the cell cycle following release from the block. We found that HCT116 cells depleted of PEA15 progress more rapidly through the cell cycle than control cells (Fig. 8C). Knockdown of *CDK6* or treatment with U0126 suppressed the cell cycle progression defect in cells depleted of PEA15 (Fig. 8C and data not shown). Depletion of *PEA15* resulted in increased colony formation, which was counteracted by the simultaneous loss of *CDK6* (Fig. 8D). Furthermore, ectopic expression of *CDK6* accelerated cell cycle progression (Fig. 8E) and led to increased colony formation in liquid culture (Fig. 8F). Collectively, these findings show that increased CDK6 expression accelerates cell cycle progression in the absence of PEA15.

PEA15 blocks RAS-mediated transformation by regulating CDK6. Oncogenic RAS mediates transformation, at least in part, by aberrantly increasing mitogen-activated protein (MAP) kinase signaling (40). Our finding that PEA15 negatively regulates MAP kinase signaling-dependent cell cycle progression prompted us to ask whether ectopic expression of PEA15 would prevent oncogenic RAS (HRAS v12)-mediated transformation. Consistent with this idea, the level of PEA15 protein was substantially reduced in HRAS v12-transformed MEFs (Fig. 9A), and ectopic expression of PEA15 inhibited HRAS v12-mediated transformation of MEFs (Fig. 9B) as well as immortalized human melanocyte MEL-ST cells (Fig. 9D and E). Similar to ectopic expression of PEA15, treatment with U0126 inhibited the transforming activity of HRAS v12 (Fig. 9B). These results suggest that suppression of PEA15 expression might be important for RAS-mediated transformation.

Based on the results described above, we asked whether the ability of PEA15 to block RAS-mediated transformation was dependent on its ability to repress *CDK6* expression. We found that ectopic expression of *CDK6* partially suppressed the PEA15-dependent inhibition of RAS-mediated transformation in both cell culture (Fig. 9B) and mouse xenografts (Fig. 9C). Collectively, these results suggest that PEA15 inhibits RAS-mediated transformation by repressing *CDK6*.

PEA15 is epigenetically silenced in human tumors. The re-

FIG 6 CDC25C is necessary for loss of the PEA15-induced DNA damage-mediated G_2/M checkpoint defect. (A) Immunoblot analysis of total ERK1/2, PEA15, and histone H1 levels in cytosolic and nuclear fractions of HCT116 cells expressing NS or *PEA15* shRNAs without or with gamma irradiation. (B) Immunoblot analysis of indicated proteins from HCT116 cells expressing NS or *PEA15* shRNAs in the presence (+) or absence (−) of the MEK inhibitor U0126. (C) Autoradiograph of ^{32}P-labeled phospho-histone H1 (p-Histone H1) after incubation with CDK1/cyclin B purified from HCT116 cells expressing NS or *PEA15* shRNAs. Immunoblots of CDK1 and cyclin B from in the inputs are also shown. (D) RT-qPCR analysis of *CDC25C* mRNA levels ($n = 3$) in HCT116 cells expressing NS or *PEA15* shRNAs with or without an additional shRNA against *CDC25C*. Error bars indicate standard errors of the means. (E) Flow cytometry analysis to measure the G_2/M checkpoint status in HCT116 cells expressing NS, *PEA15*, or *PEA15* and *CDC25C* shRNAs. Cells were analyzed at 12 h or 24 h post-gamma irradiation (p.i.). (F) Relative mitotic index after gamma irradiation of cells expressing the indicated shRNAs ($n = 3$). Error bars indicate standard errors of the means. **, $P < 0.001$. (G) Relative mitotic index after gamma irradiation of cells expressing the indicated shRNAs ($n = 3$). Error bars indicate standard errors of the means. **, $P < 0.001$.

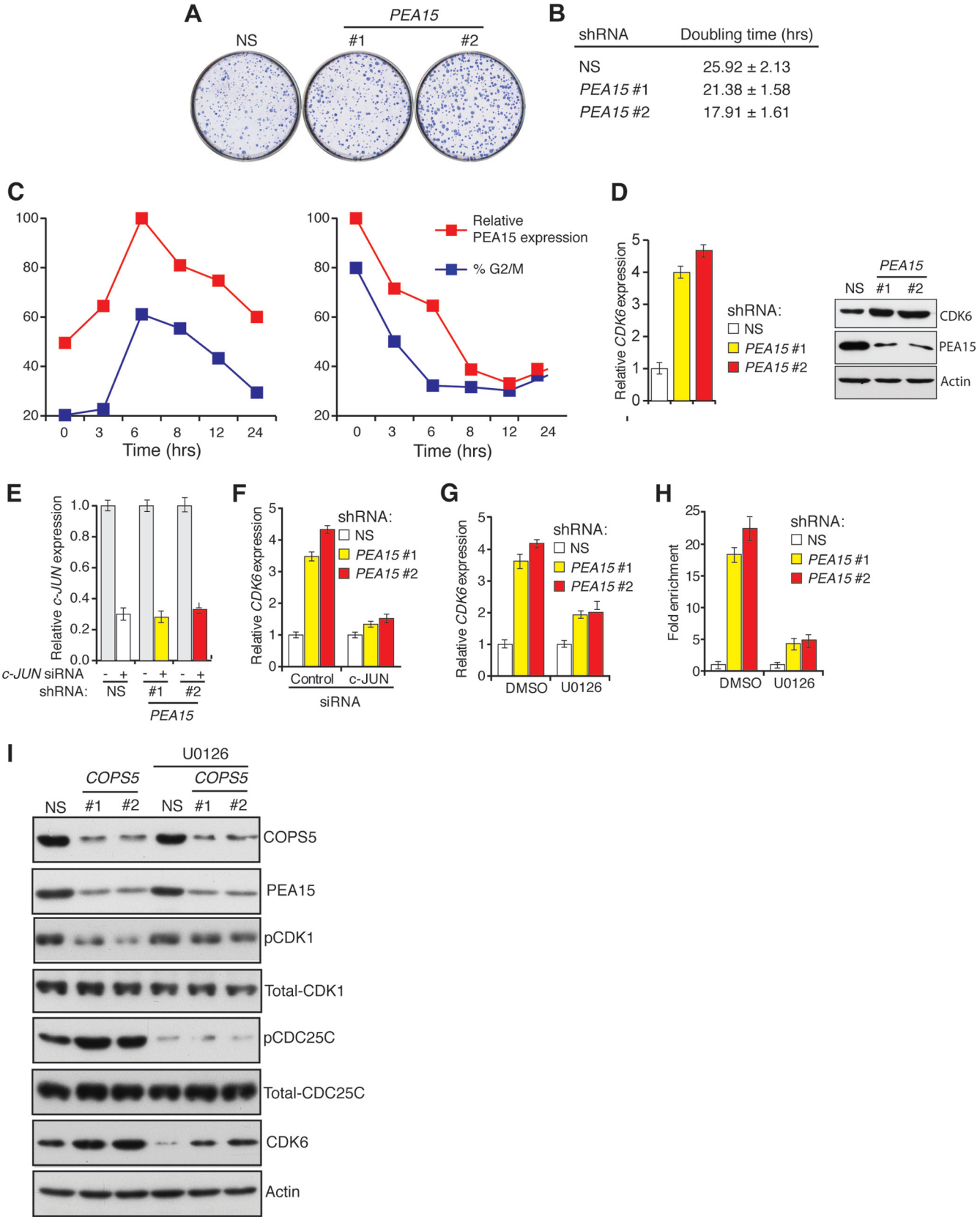

FIG 7 PEA15 regulates CDK6 transcription via transcription factor c-JUN. (A) Crystal violet staining to assay colony-forming ability of HCT116 cells expressing NS or *PEA15* (1 and 2) shRNAs. Representative wells are presented. (B) A trypan blue assay was used to determine the doubling time of HCT116 cells expressing NS or *PEA15* shRNAs. (C) Cell cycle-dependent expression of PEA15 in HCT116 cells synchronized by double thymidine block (left) or nocodazole (right).

TABLE 2 List of genes that are significantly upregulated or downregulated following shRNA-mediated knockdown of *PEA15*

Gene group and name	NCBI GeneID	Fold change in expression following *PEA15* knockdown with:[a] shRNA 1	shRNA 2
Upregulated genes			
CDK6[a]	1021	3.82	4.32
NT5E	4907	1.69	1.30
TNFRSF6B	8771	1.67	1.59
UCA1	652995	1.54	1.50
SCARNA8	677776	1.51	1.38
SNORD13	692084	1.44	1.31
TNFRSF6B	8771	1.42	1.45
SCARNA18	677765	1.40	1.31
TERC	7012	1.39	1.34
TNFRSF6B	8771	1.38	1.43
ACTA2	59	1.38	1.26
SKA2	348235	1.36	1.20
BCAR3	8412	1.33	1.42
IGFBP6	3489	1.32	1.25
AMY1C	278	1.31	1.48
SCARNA13	677768	1.30	1.51
MYEOV	26579	1.30	1.45
MALT1	10892	1.29	1.30
SDC4	6385	1.27	1.37
LDLR	3949	1.26	1.38
EPHA2	1969	1.25	1.57
NPEPPS	9520	1.24	1.24
ARPC3	10094	1.23	1.19
Downregulated genes			
DDIT4L	115265	−1.66	−1.65
PEA15	8682	−1.62	−1.97
MAP1B	4131	−1.37	−1.41
ZNF704	619279	−1.36	−1.32
MAOA	4128	−1.33	−1.26
SOX4	6659	−1.32	−1.67
ZBTB9	221504	−1.30	−1.24
LOC100133893	100133893	−1.29	−1.25
ZNF330	27309	−1.28	−1.25

[a] Fold upregulation was based on RT-qPCR validation of the microarray data.

sults described above indicate that PEA15 has many features typical of a tumor suppressor gene. Consistent with this idea, analysis of PEA15 expression by qRT-PCR revealed that *PEA15* expression was downregulated in colorectal, lung, and breast cancer samples compared to levels in the corresponding normal tissue controls (Fig. 10A).

To determine if *PEA15* is epigenetically silenced in cancers, we first used the European Bioinformatics Institute (EBI) CpG plot software to search for CpG islands in the *PEA15* promoter. This analysis identified a CpG island that spanned the promoter and first exon of *PEA15*. Methylated-DNA immunoprecipitation (Me-DIP) analyses revealed significantly higher PEA15 promoter DNA methylation in cancer samples than in the corresponding normal tissues (Fig. 10B). To further establish the role of DNA methylation-mediated epigenetic silencing in cancer samples, we performing bisulfite sequencing on a subset of colon cancer samples. This analysis confirmed that the *PEA15* promoter is hypermethylated in colon cancer samples compared to matched normal tissue (Fig. 10C). Collectively, these results show that *PEA15* expression can be epigenetically silenced due to promoter DNA hypermethylation in human tumors.

DISCUSSION

In this report, we provide several lines of evidence that document *PEA15* as a tumor suppressor gene (Fig. 10D). First, we show that after DNA damage PEA15 is stabilized by COPS5-dependent deubiquitination, which is dependent on ATM kinase activity. PEA15 protects cells from genotoxic stress-induced genomic instability by promoting the DNA damage-induced G_2/M checkpoint. Furthermore, we find that PEA15 levels oscillate throughout the cell cycle and that PEA15 expression is important for normal cell cycle progression. Finally, in further support of its role as a tumor suppressor, we find that PEA15 inhibits oncogene-induced transformation in a CDK6-dependent manner and that PEA15 is inactivated by epigenetic silencing in human tumors.

PEA15 is an integral component of the DNA damage response pathway and cell cycle machinery. The DDR pathway is a complex genetic pathway that is activated when a cell encounters genotoxic stress (41, 42). A suitable DDR pathway response to genotoxic stimuli is essential for maintaining genome integrity, preventing neoplastic transformation, and maintaining disease-free survival (41, 42). Our results show that PEA15 is an integral component of the DNA damage response pathway. We find that stabilization of PEA15 is dependent upon COPS5-mediated deubiquitination. Similar to PEA15, COPS5 is stabilized following DNA damage, which is dependent upon phosphorylation by ATM kinase but independent of its own DUB activity. It is likely that ATM-mediated phosphorylation of COSP5 at Ser320 inhibits its interaction with a putative E3 ubiquitin ligase, which consequentially prevents its polyubiquitination and proteasome-mediated degradation. Notably, we also find that COPS5-mediated deubiquitination of PEA15 is independent of its association with the CSN complex and the ability of the CSN complex to deneddylate CUL1. However, we cannot completely rule out other potential mechanisms for PEA15 stabilization following DNA damage. In response to DNA damage, PEA15 is stabilized, and we find that this stabilization is physiologically significant because loss of PEA15 results in a defective DNA damage-induced G_2/M arrest and increased mutagenesis. In addition, we find that PEA15 is also im-

PEA15 proteins levels were determined at different times following release from synchronization. PEA15 expression was determined relative to maximal expression, which was set at 100%. The percentage of cells in G_2/M phase at each time point was determined by flow cytometry. (D) RT-qPCR analysis ($n = 3$) (left) or immunoblot analysis (right) to monitor CDK6 expression in HCT116 cells expressing NS or *PEA15* shRNAs. Immunoblotting for PEA15 and actin was performed as controls. Error bars indicate standard errors of the means. (E) RT-qPCR analysis to monitor c-JUN mRNA levels in HCT116 cells expressing NS or *PEA15* shRNAs ($n = 3$) and treated with control (−) or c-*JUN* (+) siRNA. (F) RT-qPCR analysis to monitor CDK6 mRNA levels in HCT116 cells expressing NS or *PEA15* shRNAs and treated with control or c-*JUN* siRNA. Error bars indicate standard errors of the means. (G) RT-qPCR analysis to monitor *CDK6* mRNA levels ($n = 3$) in HCT116 cells expressing the indicated shRNAs and treated with 10 μM U0126 or a dimethyl sulfoxide (DMSO) control. Error bars indicate standard errors of the means. (H) c-JUN ChIP analysis at the *CDK6* promoter in HCT116 cells expressing NS or *PEA15* shRNAs and treated with a dimethyl sulfoxide control or 10 μM U0126 ($n = 3$). Error bars indicate standard errors of the means. (I) Immunoblot analysis for the indicated proteins in HCT116 cells expressing NS or *COPS5* shRNAs without or with 10 μM U0126 treatment.

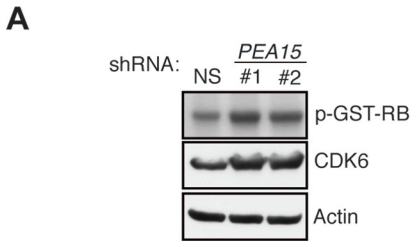
A
shRNA:
PEA15
NS
#1
#2
p-GST-RB
CDK6
Actin

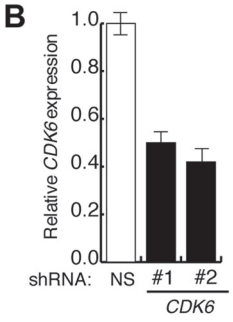
B
Relative CDK6 expression
1.0
0.8
0.6
0.4
0.2
0.0
shRNA: NS #1 #2
CDK6

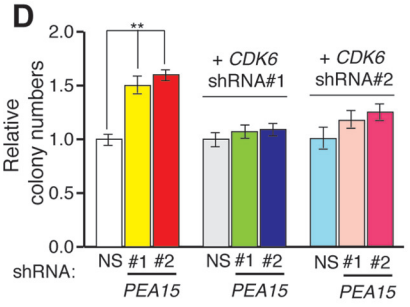
D
Relative colony numbers
2.0
1.5
1.0
0.5
0.0
**
+ CDK6 shRNA#1
+ CDK6 shRNA#2
shRNA: NS #1 #2 NS #1 #2 NS #1 #2
PEA15
PEA15
PEA15

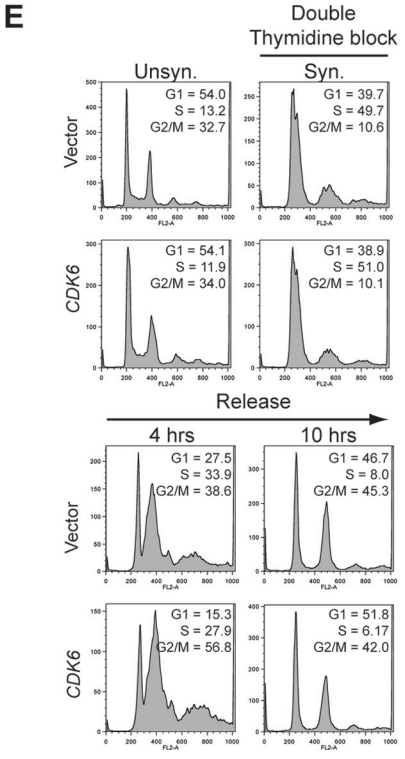
E
Double Thymidine block
Unsyn.
Syn.
Vector
G1 = 54.0
S = 13.2
G2/M = 32.7
G1 = 39.7
S = 49.7
G2/M = 10.6
CDK6
G1 = 54.1
S = 11.9
G2/M = 34.0
G1 = 38.9
S = 51.0
G2/M = 10.1
Release
4 hrs
10 hrs
Vector
G1 = 27.5
S = 33.9
G2/M = 38.6
G1 = 46.7
S = 8.0
G2/M = 45.3
CDK6
G1 = 15.3
S = 27.9
G2/M = 56.8
G1 = 51.8
S = 6.17
G2/M = 42.0

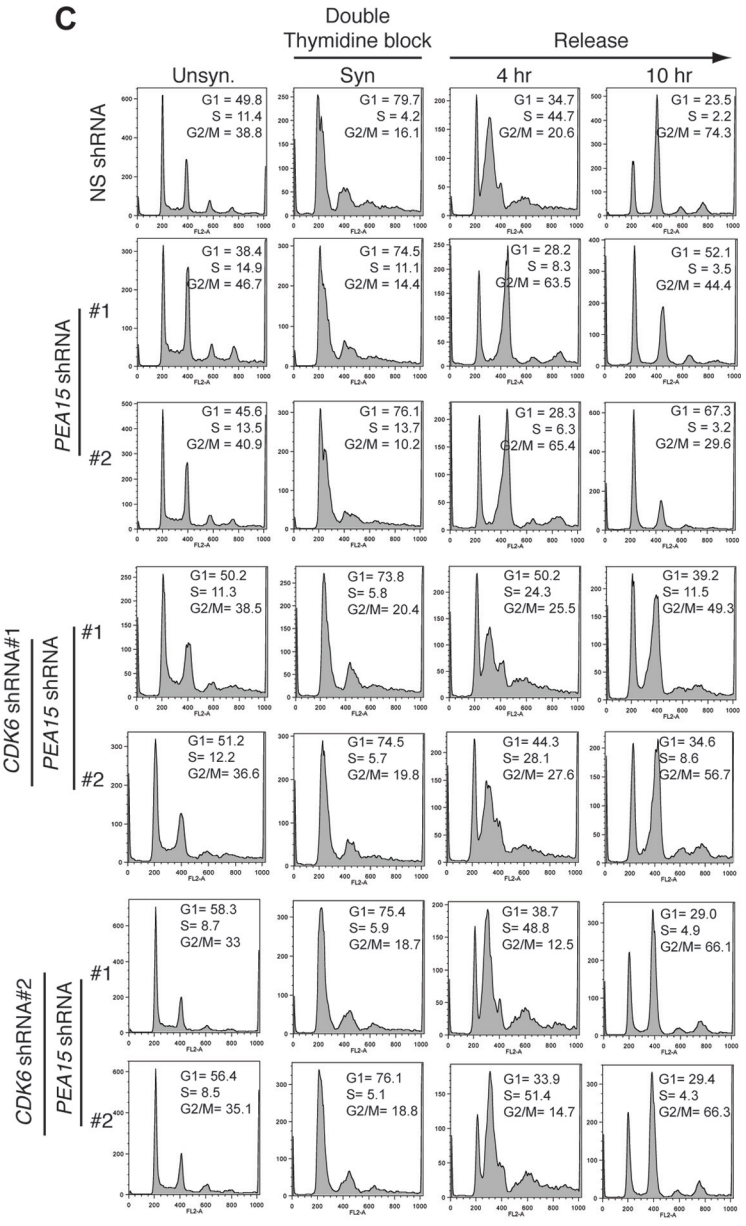
C
Double Thymidine block
Release
Unsyn.
Syn
4 hr
10 hr
NS shRNA
G1 = 49.8
S = 11.4
G2/M = 38.8
G1 = 79.7
S = 4.2
G2/M = 16.1
G1 = 34.7
S = 44.7
G2/M = 20.6
G1 = 23.5
S = 2.2
G2/M = 74.3
PEA15 shRNA #1
G1 = 38.4
S = 14.9
G2/M = 46.7
G1 = 74.5
S = 11.1
G2/M = 14.4
G1 = 28.2
S = 8.3
G2/M = 63.5
G1 = 52.1
S = 3.5
G2/M = 44.4
PEA15 shRNA #2
G1 = 45.6
S = 13.5
G2/M = 40.9
G1 = 76.1
S = 13.7
G2/M = 10.2
G1 = 28.3
S = 6.3
G2/M = 65.4
G1 = 67.3
S = 3.2
G2/M = 29.6
CDK6 shRNA#1
PEA15 shRNA #1
G1= 50.2
S= 11.3
G2/M= 38.5
G1= 73.8
S= 5.8
G2/M= 20.4
G1= 50.2
S= 24.3
G2/M= 25.5
G1= 39.2
S= 11.5
G2/M= 49.3
PEA15 shRNA #2
G1= 51.2
S= 12.2
G2/M= 36.6
G1= 74.5
S= 5.7
G2/M= 19.8
G1= 44.3
S= 28.1
G2/M= 27.6
G1= 34.6
S= 8.6
G2/M= 56.7
CDK6 shRNA#2
PEA15 shRNA #1
G1= 58.3
S= 8.7
G2/M= 33
G1= 75.4
S= 5.9
G2/M= 18.7
G1= 38.7
S= 48.8
G2/M= 12.5
G1= 29.0
S= 4.9
G2/M= 66.1
PEA15 shRNA #2
G1= 56.4
S= 8.5
G2/M= 35.1
G1= 76.1
S= 5.1
G2/M= 18.8
G1= 33.9
S= 51.4
G2/M= 14.7
G1= 29.4
S= 4.3
G2/M= 66.3

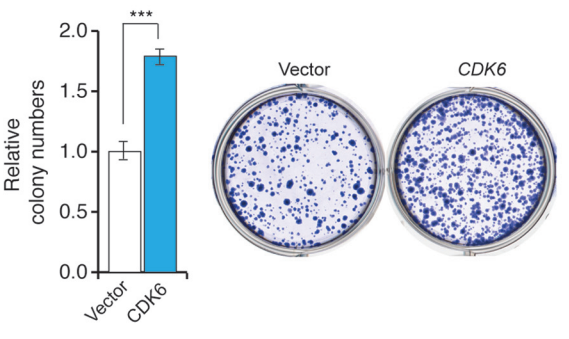
F
***
Relative colony numbers
2.0
1.5
1.0
0.5
0.0
Vector
CDK6
Vector
CDK6

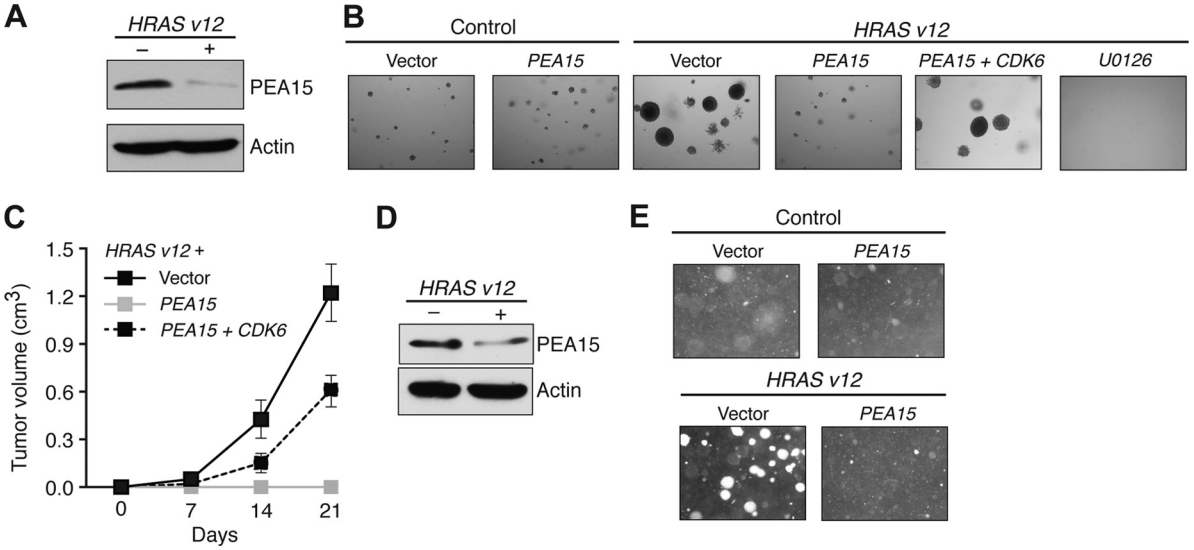

FIG 9 PEA15 inhibits RAS-induced transformation and is downregulated in multiple cancer types. (A) Immunoblot analysis of PEA15 protein from MEF/SV40-ER cells transduced with an empty or HRAS v12 expression vector. Actin expression is probed as a loading control. (B) Soft-agar assay of MEF/SV40-ER cells transduced with vectors expressing the indicated genes or treated with 10 μM U0126. Magnified images (40×) from representative wells are shown. (C) Tumorigenesis assay ($n = 5$) of MEF/SV40-ER cells expressing HRAS v12 and transduced with the indicated vectors. Tumor volumes calculated at the indicated days after injections are shown. (D) Immunoblot analysis of PEA15 levels in MEL-ST cells transduced with control (empty) or HRAS v12 expression vectors. Actin was used as a loading control. (E) Soft-agar proliferation assay of MEL-ST cells transduced with control, PEA15, HRAS v12, or both PEA15 and HRAS v12 expression vectors. Representative images are shown.

portant for normal cell cycle progression and that loss of PEA15 accelerates cell cycle progression. Mechanistically, we find that PEA15 regulates the DNA damage-induced G_2/M checkpoint through CDC25C phosphorylation and transcriptional repression of CDK6. Overall, these results reveal previously undocumented roles for PEA15 in the regulation of the DNA damage checkpoint and cell cycle regulation.

PEA15 is a regulator of cellular transformation and a tumor suppressor. Oncogenes are essential for neoplastic transformation, and intrinsic and extrinsic tumor suppression mechanisms prevent their ability to promote neoplastic transformation (43). One of the important functions of these tumor-suppressive mechanisms is to ensure genome integrity by faithfully repairing the DNA damage caused by genotoxic stress. Tumor suppressor proteins achieve this, in part, by regulating cell cycle progression and by activating the cell cycle checkpoint (7). This allows the DNA repair machinery to repair DNA and prevent accumulation and propagation of deleterious mutations. In good agreement with PEA15 as a bona fide tumor suppressor, we find that PEA15 inhibits the ability of oncogenic RAS to transform cells, which is dependent upon its ability to regulate CDK6; ectopic expression of CDK6 bypasses the ability of PEA15 to block RAS-mediated transformation. Notably, similar to PEA15, the CDK4 and CDK6 inhibitor $p15^{INK4B}$ has been shown to block RAS-mediated transformation (44), which further confirms the importance of CDK6 and other family proteins in RAS-mediated transformation.

A previous study reported that PEA15 enhanced the growth of RAS-transformed mouse kidney epithelial cells (45). However, there are many differences between that study and the experiments described here. First, we used immortalized mouse embryonic fibroblasts and immortalized melanocytes whereas the previous study used mouse kidney epithelial cells. Second, in our experiments PEA15 was introduced prior to HRAS v12, whereas in the previous study, PEA15 was introduced after HRAS v12. Therefore, whereas we were evaluating the effect of PEA15 on RAS-mediated transformation, the previous study was assessing the effect of PEA15 on RAS-transformed cells. Consistent with our results, several previous studies have shown that expression of PEA15 blocks tumor cell growth (46–48).

A number of previous studies have shown that efficient transformation of mouse and human cells by RAS is dependent upon downstream signaling through the ERK pathway (40, 49). PEA15

FIG 8 Loss of PEA15 accelerates cell cycle progression via CDK6. (A) Autoradiograph of ^{32}P-labeled GST-RB after incubation with CDK6 purified from HCT116 cells expressing NS or PEA15 (1 and 2) shRNAs. Immunoblots of CDK6 and actin from the whole-cell lysates are also shown. (B) RT-qPCR analysis for monitoring CDK6 expression in HCT116 cells expressing the indicated shRNAs ($n = 3$). Error bars indicate standard errors of the means. (C) Flow cytometry to determine the cell cycle distribution of HCT116 cells expressing NS or *PEA15* shRNAs or expressing shRNAs for both *PEA15* shRNAs and *CDK6* shRNA. The percentage of cells in each stage of the cell cycle is indicated for unsynchronized (Unsyn) cells, cells synchronized (Syn) by double thymidine block, and cells collected at the indicated time points after release from double thymidine block. (D) Colony formation assay for HCT116 cells expressing NS or *PEA15* shRNAs in the presence or absence of *CDK6* shRNA ($n = 3$). Error bars indicate standard errors of the means. (E) Flow cytometry analyses to determine the cell cycle distribution of HCT116 cells stably transduced with control or *CDK6* expression vectors. The percentage of cells in each stage of the cell cycle is indicated for unsynchronized (Unsyn) cells, synchronized (Syn) cells arrested in G_1 by double thymidine block, and cells released from arrest for the indicated time. (F) Colony formation assay for HCT116 cells expressing vector or *CDK6*. Relative colony numbers under the indicated conditions are indicated (left), and a representative crystal violet-stained wells are shown (right). Error bars indicate standard errors of the means. **, $P < 0.001$.

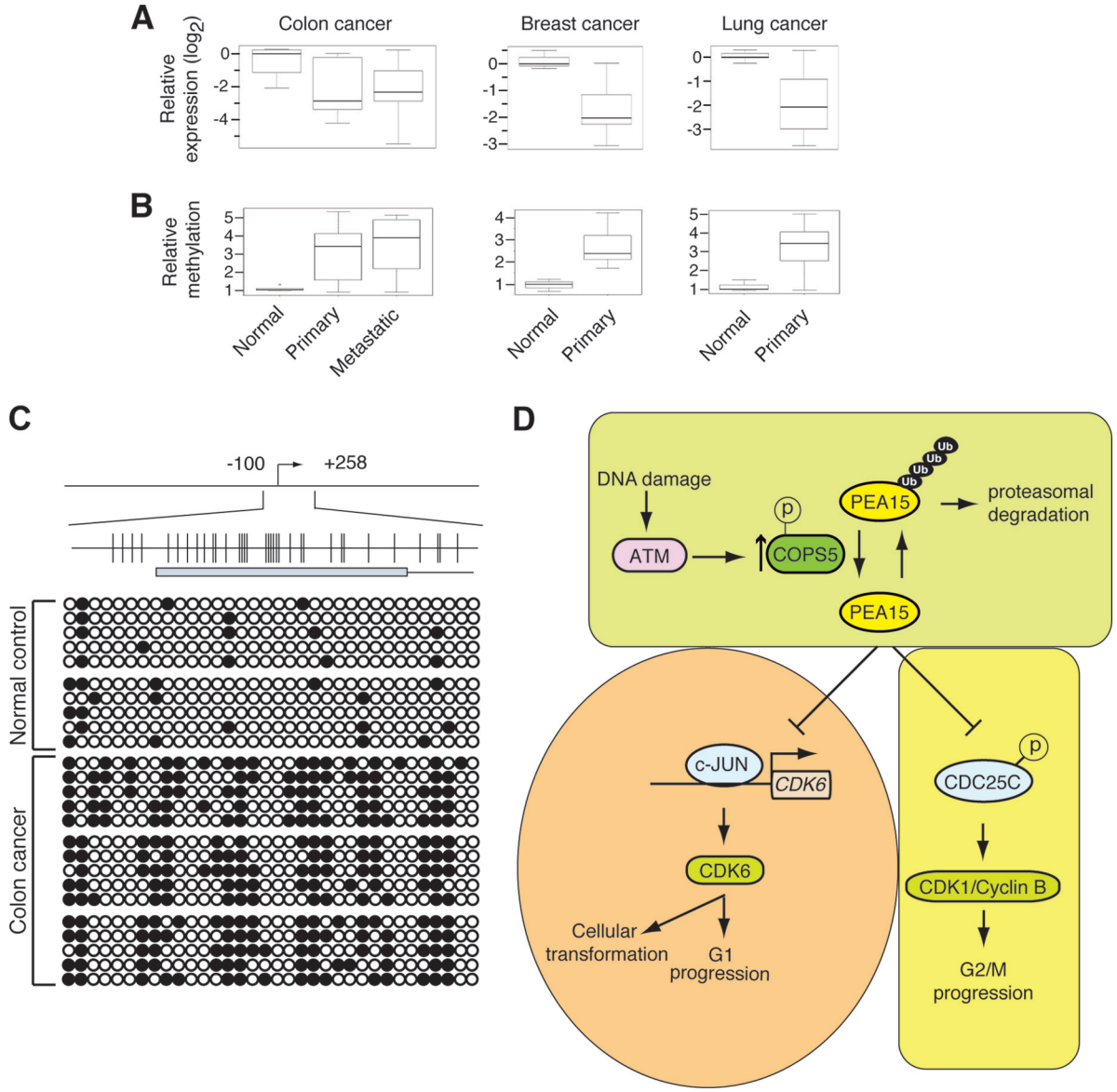

FIG 10 PEA15 is epigenetically silenced due to promoter DNA methylation in patient-derived tumor samples. (A) RT-qPCR analysis of *PEA15* mRNA levels in normal ($n = 5$) and primary tumor ($n = 10$) or metastatic tumor ($n = 10$) samples from colon, breast, or lung. The normal data point is an average of five samples. (B) Relative *PEA15* methylation level analyses by Me-DIP in normal and primary tumor or metastatic tumor samples from colon, breast, or lung. The normal data point is an average of five samples. (C) Bisulfite sequencing analysis of *PEA15* promoter methylation in normal and colon cancer samples. (D) Model.

sequesters ERK in the cytoplasm, thus preventing ERK from phosphorylating its nuclear targets. An attractive explanation for our finding that PEA15 blocks RAS-mediated transformation is the loss of nuclear ERK-driven phosphorylation. Consistent with this idea, a previous study reported that in cells undergoing RAS-induced senescence, ERK is predominately cytoplasmic (50). However, coexpression of the oncoprotein E1A, which causes bypass of RAS-induced senescence, restores nuclear ERK localization (50). Our results, in conjunction with these previous studies, show that PEA15 is an important regulator of RAS-mediated transformation. It will be interesting to determine whether PEA15 will also block transformation by other oncogenes, such as BRAF and epidermal growth factor receptor (EGFR), which also regulated ERK signaling to induce cellular transformation.

ACKNOWLEDGMENTS

We thank Angelika Amon and Mark Hochstrasser for helpful discussions and David Stern for his useful comments on the manuscript. We thank Darryl Conte for editorial assistance.

N.W. is a translational scholar of the Sidney Kimmel Foundation for Cancer Research and is supported by a Young Investigator Award from the National Lung Cancer Partnership, Uniting against Lung Cancer, and the International Association for the Study of Lung Cancer, Melanoma Research Alliance and Melanoma Research Foundation. M.R.G. is an investigator of the Howard Hughes Medical Institute. This work was supported in part by a grant from the NIH (R01GM033977) to M.R.G.

REFERENCES

1. **Lowe SW, Cepero E, Evan G.** 2004. Intrinsic tumour suppression. Nature **432**:307–315. http://dx.doi.org/10.1038/nature03098.

2. **Yaswen P, Campisi J.** 2007. Oncogene-induced senescence pathways weave an intricate tapestry. Cell **128:**233–234. http://dx.doi.org/10.1016/j.cell.2007.01.005.
3. **Rodier F, Campisi J.** 2011. Four faces of cellular senescence. J. Cell Biol. **192:**547–556. http://dx.doi.org/10.1083/jcb.201009094.
4. **Di Micco R, Fumagalli M, Cicalese A, Piccinin S, Gasparini P, Luise C, Schurra C, Garre M, Nuciforo PG, Bensimon A, Maestro R, Pelicci PG, d'Adda di Fagagna F.** 2006. Oncogene-induced senescence is a DNA damage response triggered by DNA hyper-replication. Nature **444:**638–642. http://dx.doi.org/10.1038/nature05327.
5. **Bartkova J, Rezaei N, Liontos M, Karakaidos P, Kletsas D, Issaeva N, Vassiliou LV, Kolettas E, Niforou K, Zoumpourlis VC, Takaoka M, Nakagawa H, Tort F, Fugger K, Johansson F, Sehested M, Andersen CL, Dyrskjot L, Orntoft T, Lukas J, Kittas C, Helleday T, Halazonetis TD, Bartek J, Gorgoulis VG.** 2006. Oncogene-induced senescence is part of the tumorigenesis barrier imposed by DNA damage checkpoints. Nature **444:**633–637. http://dx.doi.org/10.1038/nature05268.
6. **Lujambio A, Akkari L, Simon J, Grace D, Tschaharganeh DF, Bolden JE, Zhao Z, Thapar V, Joyce JA, Krizhanovsky V, Lowe SW.** 2013. Non-cell-autonomous tumor suppression by p53. Cell **153:**449–460. http://dx.doi.org/10.1016/j.cell.2013.03.020.
7. **Bunz F, Dutriaux A, Lengauer C, Waldman T, Zhou S, Brown JP, Sedivy JM, Kinzler KW, Vogelstein B.** 1998. Requirement for p53 and p21 to sustain G_2 arrest after DNA damage. Science **282:**1497–1501. http://dx.doi.org/10.1126/science.282.5393.1497.
8. **Morgan SE, Kastan MB.** 1997. p53 and ATM: cell cycle, cell death, and cancer. Adv. Cancer Res. **71:**1–25. http://dx.doi.org/10.1016/S0065-230X(08)60095-0.
9. **Wajapeyee N, Serra RW, Zhu X, Mahalingam M, Green MR.** 2008. Oncogenic BRAF induces senescence and apoptosis through pathways mediated by the secreted protein IGFBP7. Cell **132:**363–374. http://dx.doi.org/10.1016/j.cell.2007.12.032.
10. **Fiory F, Formisano P, Perruolo G, Beguinot F.** 2009. Frontiers: PED/PEA-15, a multifunctional protein controlling cell survival and glucose metabolism. Am. J. Physiol. Endocrinol. Metab. **297:**E592–E601. http://dx.doi.org/10.1152/ajpendo.00228.2009.
11. **Formstecher E, Ramos JW, Fauquet M, Calderwood DA, Hsieh JC, Canton B, Nguyen XT, Barnier JV, Camonis J, Ginsberg MH, Chneiweiss H.** 2001. PEA-15 mediates cytoplasmic sequestration of ERK MAP kinase. Dev. Cell **1:**239–250. http://dx.doi.org/10.1016/S1534-5807(01)00035-1.
12. **Schmittgen TD, Livak KJ.** 2008. Analyzing real-time PCR data by the comparative C(T) method. Nat. Protoc. **3:**1101–1108. http://dx.doi.org/10.1038/nprot.2008.73.
13. **Raha T, Cheng SW, Green MR.** 2005. HIV-1 Tat stimulates transcription complex assembly through recruitment of TBP in the absence of TAFs. PLoS Biol. **3:**e44. http://dx.doi.org/10.1371/journal.pbio.0030044.
14. **Santra MK, Wajapeyee N, Green MR.** 2009. F-box protein FBXO31 mediates cyclin D1 degradation to induce G_1 arrest after DNA damage. Nature **459:**722–725. http://dx.doi.org/10.1038/nature08011.
15. **Whitfield ML, Sherlock G, Saldanha AJ, Murray JI, Ball CA, Alexander KE, Matese JC, Perou CM, Hurt MM, Brown PO, Botstein D.** 2002. Identification of genes periodically expressed in the human cell cycle and their expression in tumors. Mol. Biol. Cell **13:**1977–2000. http://dx.doi.org/10.1091/mbc.02-02-0030..
16. **Hurov KE, Cotta-Ramusino C, Elledge SJ.** 2010. A genetic screen identifies the Triple T complex required for DNA damage signaling and ATM and ATR stability. Genes Dev. **24:**1939–1950. http://dx.doi.org/10.1101/gad.1934210.
17. **Fang M, Xia F, Mahalingam M, Virbasius CM, Wajapeyee N, Green MR.** 2013. MEN1 is a melanoma tumor suppressor that preserves genomic integrity by stimulating transcription of genes that promote homologous recombination-directed DNA repair. Mol. Cell. Biol. **33:**2635–2647. http://dx.doi.org/10.1128/MCB.00167-13.
18. **Shan J, Zhao W, Gu W.** 2009. Suppression of cancer cell growth by promoting cyclin D1 degradation. Mol. Cell **36:**469–476. http://dx.doi.org/10.1016/j.molcel.2009.10.018.
19. **MacLachlan TK, Somasundaram K, Sgagias M, Shifman Y, Muschel RJ, Cowan KH, El-Deiry WS.** 2000. BRCA1 effects on the cell cycle and the DNA damage response are linked to altered gene expression. J. Biol. Chem. **275:**2777–2785. http://dx.doi.org/10.1074/jbc.275.4.2777.
20. **Canman CE, Lim DS, Cimprich KA, Taya Y, Tamai K, Sakaguchi K, Appella E, Kastan MB, Siliciano JD.** 1998. Activation of the ATM kinase by ionizing radiation and phosphorylation of p53. Science **281:**1677–1679. http://dx.doi.org/10.1126/science.281.5383.1677.
21. **Du P, Kibbe WA, Lin SM.** 2008. lumi: a pipeline for processing Illumina microarray. Bioinformatics **24:**1547–1548. http://dx.doi.org/10.1093/bioinformatics/btn224.
22. **Smyth GK.** 2004. Linear models and empirical bayes methods for assessing differential expression in microarray experiments. Stat. Appl. Genet. Mol. Biol. **3:**Article3. http://dx.doi.org/10.2202/1544-6115.1027.
23. **Benjamini Y, Hochberg Y.** 1995. Controlling the false discovery rate: a practical and powerful approach to multiple testing. J. R. Stat. Soc. Series B Stat. Methodol. **57:**289–300.
24. **Weber M, Davies JJ, Wittig D, Oakeley EJ, Haase M, Lam WL, Schubeler D.** 2005. Chromosome-wide and promoter-specific analyses identify sites of differential DNA methylation in normal and transformed human cells. Nat. Genet. **37:**853–862. http://dx.doi.org/10.1038/ng1598.
25. **Shieh SY, Ikeda M, Taya Y, Prives C.** 1997. DNA damage-induced phosphorylation of p53 alleviates inhibition by MDM2. Cell **91:**325–334. http://dx.doi.org/10.1016/S0092-8674(00)80416-X.
26. **Wei N, Deng XW.** 2003. The COP9 signalosome. Annu. Rev. Cell Dev. Biol. **19:**261–286. http://dx.doi.org/10.1146/annurev.cellbio.19.111301.112449.
27. **Liu Y, Shah SV, Xiang X, Wang J, Deng ZB, Liu C, Zhang L, Wu J, Edmonds T, Jambor C, Kappes JC, Zhang HG.** 2009. COP9-associated CSN5 regulates exosomal protein deubiquitination and sorting. Am. J. Pathol. **174:**1415–1425. http://dx.doi.org/10.2353/ajpath.2009.080861.
28. **Chamovitz DA, Segal D.** 2001. JAB1/CSN5 and the COP9 signalosome. A complex situation. EMBO Rep. **2:**96–101. http://dx.doi.org/10.1093/embo-reports/kve028.
29. **Matsuoka S, Ballif BA, Smogorzewska A, McDonald ER, 3rd, Hurov KE, Luo J, Bakalarski CE, Zhao Z, Solimini N, Lerenthal Y, Shiloh Y, Gygi SP, Elledge SJ.** 2007. ATM and ATR substrate analysis reveals extensive protein networks responsive to DNA damage. Science **316:**1160–1166. http://dx.doi.org/10.1126/science.1140321.
30. **Bemis L, Chan DA, Finkielstein CV, Qi L, Sutphin PD, Chen X, Stenmark K, Giaccia AJ, Zundel W.** 2004. Distinct aerobic and hypoxic mechanisms of HIF-alpha regulation by CSN5. Genes Dev. **18:**739–744. http://dx.doi.org/10.1101/gad.1180104.
31. **Cope GA, Deshaies RJ.** 2003. COP9 signalosome: a multifunctional regulator of SCF and other cullin-based ubiquitin ligases. Cell **114:**663–671. http://dx.doi.org/10.1016/S0092-8674(03)00722-0.
32. **Wei N, Serino G, Deng XW.** 2008. The COP9 signalosome: more than a protease. Trends Biochem. Sci. **33:**592–600. http://dx.doi.org/10.1016/j.tibs.2008.09.004.
33. **Wolf DA, Zhou C, Wee S.** 2003. The COP9 signalosome: an assembly and maintenance platform for cullin ubiquitin ligases? Nat. Cell Biol. **5:**1029–1033. http://dx.doi.org/10.1038/ncb1203-1029.
34. **Lyapina S, Cope G, Shevchenko A, Serino G, Tsuge T, Zhou C, Wolf DA, Wei N, Deshaies RJ.** 2001. Promotion of NEDD-CUL1 conjugate cleavage by COP9 signalosome. Science **292:**1382–1385. http://dx.doi.org/10.1126/science.1059780.
35. **Zhou BB, Elledge SJ.** 2000. The DNA damage response: putting checkpoints in perspective. Nature **408:**433–439. http://dx.doi.org/10.1038/35044005.
36. **Wang R, He G, Nelman-Gonzalez M, Ashorn CL, Gallick GE, Stukenberg PT, Kirschner MW, Kuang J.** 2007. Regulation of Cdc25C by ERK-MAP kinases during the G_2/M transition. Cell **128:**1119–1132. http://dx.doi.org/10.1016/j.cell.2006.11.053.
37. **Strausfeld U, Labbe JC, Fesquet D, Cavadore JC, Picard A, Sadhu K, Russell P, Doree M.** 1991. Dephosphorylation and activation of a p34cdc2/cyclin B complex in vitro by human CDC25 protein. Nature **351:**242–245. http://dx.doi.org/10.1038/351242a0.
38. **Boutros R, Lobjois V, Ducommun B.** 2007. CDC25 phosphatases in cancer cells: key players? Good targets? Nat. Rev. Cancer **7:**495–507. http://dx.doi.org/10.1038/nrc2169.
39. **Leppa S, Saffrich R, Ansorge W, Bohmann D.** 1998. Differential regulation of c-Jun by ERK and JNK during PC12 cell differentiation. EMBO J. **17:**4404–4413. http://dx.doi.org/10.1093/emboj/17.15.4404.
40. **Hamad NM, Elconin JH, Karnoub AE, Bai W, Rich JN, Abraham RT, Der CJ, Counter CM.** 2002. Distinct requirements for Ras oncogenesis in human versus mouse cells. Genes Dev. **16:**2045–2057. http://dx.doi.org/10.1101/gad.993902.
41. **Harper JW, Elledge SJ.** 2007. The DNA damage response: ten years after. Mol. Cell **28:**739–745. http://dx.doi.org/10.1016/j.molcel.2007.11.015.

42. **Ciccia A, Elledge SJ.** 2010. The DNA damage response: making it safe to play with knives. Mol. Cell **40:**179–204. http://dx.doi.org/10.1016/j.molcel.2010.09.019.
43. **Campisi J.** 2001. Cellular senescence as a tumor-suppressor mechanism. Trends Cell Biol. **11:**S27–S31. http://dx.doi.org/10.1016/S0962-8924(01)82148-6.
44. **Malumbres M, Perez De Castro I, Hernandez MI, Jimenez M, Corral T, Pellicer A.** 2000. Cellular response to oncogenic ras involves induction of the Cdk4 and Cdk6 inhibitor $p15^{INK4b}$. Mol. Cell. Biol. **20:**2915–2925. http://dx.doi.org/10.1128/MCB.20.8.2915-2925.2000.
45. **Sulzmaier FJ, Valmiki MK, Nelson DA, Caliva MJ, Geerts D, Matter ML, White EP, Ramos JW.** 2012. PEA-15 potentiates H-Ras-mediated epithelial cell transformation through phospholipase D. Oncogene **31:**3547–3560. http://dx.doi.org/10.1038/onc.2011.514.
46. **Glading A, Koziol JA, Krueger J, Ginsberg MH.** 2007. PEA-15 inhibits tumor cell invasion by binding to extracellular signal-regulated kinase 1/2. Cancer Res. **67:**1536–1544. http://dx.doi.org/10.1158/0008-5472.CAN-06-1378.
47. **Bartholomeusz C, Gonzalez-Angulo AM, Kazansky A, Krishnamurthy S, Liu P, Yuan LX, Yamasaki F, Liu S, Hayashi N, Zhang D, Esteva FJ, Hortobagyi GN, Ueno NT.** 2010. PEA-15 inhibits tumorigenesis in an MDA-MB-468 triple-negative breast cancer xenograft model through increased cytoplasmic localization of activated extracellular signal-regulated kinase. Clin. Cancer Res. **16:**1802–1811. http://dx.doi.org/10.1158/1078-0432.CCR-09-1456.
48. **Bartholomeusz C, Rosen D, Wei C, Kazansky A, Yamasaki F, Takahashi T, Itamochi H, Kondo S, Liu J, Ueno NT.** 2008. PEA-15 induces autophagy in human ovarian cancer cells and is associated with prolonged overall survival. Cancer Res. **68:**9302–9310. http://dx.doi.org/10.1158/0008-5472.CAN-08-2592.
49. **Rangarajan A, Hong SJ, Gifford A, Weinberg RA.** 2004. Species- and cell type-specific requirements for cellular transformation. Cancer Cell **6:**171–183. http://dx.doi.org/10.1016/j.ccr.2004.07.009.
50. **Gaumont-Leclerc MF, Mukhopadhyay UK, Goumard S, Ferbeyre G.** 2004. PEA-15 is inhibited by adenovirus E1A and plays a role in ERK nuclear export and Ras-induced senescence. J. Biol. Chem. **279:**46802–46809. http://dx.doi.org/10.1074/jbc.M403893200.